An analytical phytoplankton model and its application in the tidal freshwater James River

Zhengui Wang^{1,*}, Harry Wang², Jian Shen², Fei Ye², Yinglong Zhang², Fei Chai¹, Zhuo Liu³, Jiabi Du⁴

Corresponding author

Name: Zhengui Wang

Email: wzhengui@gmail.com

Address: Room 452, 5706 Aubert Hall, Orono, ME 04469-5706

Keywords:

analytical model
phytoplankton dynamics
physical transport
biological processes
physical mixing
nonlinear term

Funding Support: DOE project 'Improving tide-estuary representation in MPAS-Ocean' with program grant number DE-SC0016263 (to Zhang Yinglong at Virginia Institute of Marine Sciences).

Declaration: All authors agree to the submission of this manuscript

¹ School of Marine Sciences, University of Maine, Orono, ME 04469, USA

² Virginia Institute of Marine Science, College of William & Mary, Center for Coastal Resource Management, 1375 Greate Road, Gloucester Point, VA 23062, USA

³ Texas Water Development Board, Austin, TX 78701, USA

⁴ Texas A&M University at Galveston, Galveston, TX 77554, USA

Abstract

1

2

3

4

5

6

7

8

9

10

11

12

13

14

15

16 17

18

19

This study constructs an analytical model to understand the phytoplankton dynamics in a onedimensional system by integrating the physical and biological processes. We present an analytical solution of phytoplankton distribution along the longitudinal direction of a tidal river. The solution has two components: water age and accumulative growth. The water age represents the overall effect of physical transport due to advection, while the accumulative growth represents the accumulation of phytoplankton biomass due to biological processes during the transport. In addition, an alternative solution with nonlinear reaction term is given to account for the feedback mechanism of nonlinear processes that affect phytoplankton growth rate. The nonlinear reaction term can be also used to approximate the effect of physical mixing on phytoplankton distribution. The analytical solutions can be further used to predict the temporal variation and spatial distribution of phytoplankton along the tidal river. They also serve as a mathematical tool to unite different field phytoplankton observations. We applied the model in the Tidal Freshwater Region (TFR) of James River under different dynamic conditions and the model results match well with the observations, which validates the theory on different time scales. Furthermore, an analysis is conducted for the Local Chlorophyll-a Maximum (LCM) in the TFR. It shows that the condition for LCM is biologically controlled, but its location is regulated by river flow and river geomorphology.

1 Introduction

20

48

49

TFR is a part of an estuary that is under heavy influence of tide and river flow, but beyond the 21 influence of saline water. Due to the strong mixing, it is usually a well-mixed system (Cloern, 22 1987; Wood et al., 2013). Watershed runoff brings nutrients into TFR resulting in high nutrient 23 concentration conditions that can support high primary production (Carroll et al., 2013; Heisler et 24 al., 2008). Therefore, phytoplankton blooms are often observed in TFR (Filardo & Dunstan, 1985; 25 James et al., 1992; Muylaert et al., 2005), which could pose threat to the ecosystem (Anderson et 26 27 al., 2012; Bukaveckas et al., 2011; Cloern, 1996). Phytoplankton growth in TFR is related to many 28 factors, including nutrients, light, temperature and grazing (Cloern, 1987; Dugdale et al., 2016; James et al., 1992; Marshall & Affronti, 1992; Qin & Shen, 2017; Sellner et al., 1988). Besides, 29 the river flow plays an important role in the phytoplankton dynamics in TFR by influencing the 30 residence time and spatial distribution of phytoplankton (Borsuk et al., 2004; Bukaveckas et al., 31 2011; Lucas et al., 2009). The interaction between the physical and biological controls on 32 phytoplankton dynamics is the key for us to interpret the ecosystem features in TFR such as the 33 chlorophyll maximum (Bukaveckas et al., 2011). In estuaries, physical transport and 34 phytoplankton growth are both well studied (Glibert et al., 2001; Hong & Shen, 2013; Ralston et 35 al., 2015; Shen & Lin, 2006), and these studies provide insights to the coupling between these two 36 elements in TFR. However, if we only focus on the biological behaviors of phytoplankton, we lose 37 the overall picture of its spatial distribution and connections between upstream and downstream. 38 On the other hand, if we only study the physical transport, it is insufficient to understand the 39 complex biological response of phytoplankton to environmental factors. The goal of this work is 40 41 to integrate the physical and biological processes to understand the phytoplankton dynamics in TFR. 42 For physical transport process, timescale is a useful tool to represent its bulk effect on the 43 44 ecosystem (Deleersnijder et al., 2001; Shen et al., 2013). The comparison between the timescale of physical transport and the timescale of biological processes depicts their relative importance in 45 46 regulating the ecosystem. Using transit time and the timescale of algal growth, Lucas et al. (2009) 47 studied the relationship between phytoplankton biomass and transport time in different estuaries.

Based on the timescales of gravitational circulation, vertical exchange and total oxygen

consumption, Shen et al. (2013) and Du and Shen (2015) studied the dissolved oxygen distribution

in Chesapeake Bay. To understand the complex water flows, Deleersnijder et al. (2001) introduced the concept of water age to diagnose the underlying physical processes using timescales. The water age is the time elapsed since the water parcel left the considered region. The water age is a function of time and location and it represents the history of the water parcel by relating it to its original location where the age is set to zero. This concept provides a robust tool for us to interpret the hydrodynamic process in an aquatic system, as it not only relates the information of water parcels in different places (Shen & Lin, 2006) but also shows the accumulating effect of flow history. In this study, we integrate water age into the phytoplankton dynamics to analyze the effect of physical transport on spatial and temporal variations of phytoplankton.

To describe the phytoplankton behaviors in a waterbody, various biological processes are often characterized by different rates such as growth rate, respiration rate, grazing rate, etc. (Boynton et al., 1982; Cerco & Noel, 2004; Liu et al., 2018; Morse et al., 2013; Park et al., 1995). These rates represent the rates of different processes in changing the phytoplankton biomass and each is inherited with a timescale in an inverse relationship. Normally, high rate implies a short timescale and a large influence on the phytoplankton. To study the mass balance of phytoplankton biomass, different rates can be lumped into two terms (Lucas et al., 2009): growth rate that summaries all the rates of increasing phytoplankton biomass such as the photosynthesis rate and phagocytic rate for mixotrophic species (Flynn & Mitra, 2009), and loss rate that summaries all the rates of decreasing phytoplankton biomass such as respiration rate and grazing rate. By comparing growth rate and loss rate, we can know whether phytoplankton biomass will increase or not with time. In addition, these two rates reveal the changing rate of phytoplankton concentration in an aquatic system relative to the physical transport. Phytoplankton net growth rate can be further defined as the growth rate subtracted by the loss rate (Lucas et al., 2009). Moreover, growth and loss rates can both vary with time and space because of the responses of phytoplankton to varying environmental conditions, which substantially increases the difficulty in studying phytoplankton dynamics.

Because growth and loss rates may change in different location, essentially, their effects on phytoplankton are locally defined focusing on the phytoplankton biological behaviors in individual places (Anderson et al., 2008). These rates are not able to provide the bulk effect on phytoplankton that accumulated in time and space. In addition, they cannot give the information about the relation between phytoplankton in different places even the water parcels of phytoplankton are physically

related. In order to integrate the biological rates with physical transport, Lucas et al. (2009) developed a conceptual phytoplankton model for a one-dimensional, uniform and steady state system. This model considers the phytoplankton concentrations that go in and out a system by comparing the physical and biological timescales. Basically, it shows that phytoplankton concentration increases/decreases through time during physical transit, when growth rate is larger/smaller than loss rate. Phytoplankton is regarded as passive tracers conveyed by the water parcel. In the system, phytoplankton grows or decays with time depending on the sign of the net growth rate. In the meantime, water parcel flow through the system, e.g., from the head to the end of an estuary. From a Lagrangian point of view, time and space are tightly coupled for the phytoplankton in a particular water parcel. Therefore, when phytoplankton are transported in a certain distance, the phytoplankton also spends a certain time for their biological changes.

81

82

83

84

85 86

87

88 89

90

91

92

93

94

95

96 97

98

99

100

101102

103

104

105

106

107

108

109

110

111

Generally, field measurements for phytoplankton concentrations can be divided into two categories: the first category focuses on the time series at a fixed location lacking enough spatial resolution and the second category focuses on the spatial variation at a specific time lacking enough temporal resolution (Chesapeake Bay Program, 2016). It is not practical to obtain phytoplankton measurements with both high temporal and spatial resolutions. To fill the data gap, efforts have been made to integrate different kinds of observations to understand the physical and biological controls on phytoplankton dynamics (Cianelli et al., 2017; Qin & Shen, 2017). Models (either analytical or numerical) are also used to estimate the phytoplankton concentration at the vacancy of measurements. Lucas's phytoplankton model is sufficient to describe a simple steady water system (Lucas et al., 2009). However, it may fail to capture the phytoplankton variations in a varying system. In this work, we present a more generic analytical phytoplankton model that can analyze the phytoplankton variation when biological rates and physical transit time are both changing with time and space. Mathematically, it is composed of two components: one responsible for the physical transport (water age) and the other responsible for the accumulation of biological effects. This model provides a tool to unite different kinds of phytoplankton measurements regarding its spatiotemporal variations. It has the potential of predicting one from the other if only one kind of measurement is available. Thus, it can also be used to check the consistence between them. Different from numerical models, what we derived in this study is an analytical solution to the equation of phytoplankton dynamics, which can be used in many areas including: 1) predicting phytoplankton variation in time and space, 2) integrating the biological and physical factors that affect phytoplankton variations, 3) building a relation between temporal variation and spatial variation of phytoplankton, and 4) theoretically analyzing phytoplankton phenomenon. In this work, we apply this new model in the TFR of James River located in the lower Chesapeake Bay to predict the temporal and spatial phytoplankton variations.

2 Method

To simulate chlorophyll spatiotemporal variations in estuaries, numerical modeling is the most popular method by coupling a biological model of phytoplankton growth with a hydrodynamics model (Cerco, 2013; Liu et al., 2018; Park et al., 1995; Shen et al., 2017). In addition, empirical models are also often used by statistically linking the phytoplankton variations with environmental factors (Chesapeake Environmental Communications, 2015; Fitzpatrick et al., 2014; Shen et al., 2016a). These methods are usually focused on the long-term variabilities of chlorophyll compared with monthly or semi-monthly observations (Cerco & Noel, 2004; Chesapeake Bay Program, 2016). In this study, we adopt a new approach by directly deriving the analytical solution to the equations of phytoplankton dynamics. Then, evaluation of the solution can reproduce downstream chlorophyll variations.

2.1 Phytoplankton Dynamics without diffusivity

Many TFRs can be described by a one-dimensional system that is homogenous in the cross section. The river flow generally varies longitudinally with time. If the diffusivity effect can be neglected, water parcels are simply advected from upstream to downstream (Lucas et al., 2009; Shen et al., 1999). For these types of water system, the phytoplankton dynamics can be expressed in the following equation along with a boundary condition:

$$\frac{\partial C}{\partial t} + u \frac{\partial C}{\partial x} = \left(\mu_{growth} - \mu_{loss}\right) \cdot C = \mu_{net} \cdot C \quad , \text{ for } x \in [0, L]$$
(1)

 $C(t, x=0) = a(t), \tag{2}$

where C(t,x) (mg/L) is phytoplankton biomass which can also be represented by chlorophyll concentration in the unit of μ g[Chl]/L; t is time; x is the downstream distance from the river head; u(t,x) (m/s) is velocity; μ_{growth} and μ_{loss} are phytoplankton growth and loss rate respectively;

 $\mu_{net}(t,x)$ is the net growth rate and L is the length of TFR. In addition, a(t) is the boundary condition for phytoplankton concentration located at the river head and it varies with time. Note both u(t,x) and $\mu_{net}(t,x)$ are varying with time and space. $\frac{\partial C}{\partial t}$ represents the local changing rate of phytoplankton biomass, which is controlled by two processes. First, phytoplankton is transported by the river flow with a velocity u. Second, phytoplankton concentration is changing along the transport at the rate of $\mu_{\scriptscriptstyle net}$. Here, phytoplankton in the system [0,L] is assumed to originate from the upstream at x = 0 and there is no local sources such as benthic resuspension (Kemp & Boynton, 1992).

The solution to Equations (1-2) is

$$C(t,x) = a(t-T) \cdot e^{G} \quad \text{, for } x \in [0, L]$$

where T(t,x) and G(t,x) are implicitly expressed by the equations below:

$$\frac{\partial T}{\partial t} + u \frac{\partial T}{\partial x} = 1 \tag{4}$$

$$\frac{\partial G}{\partial t} + u \frac{\partial G}{\partial x} = \mu_{net} \tag{5}$$

$$T(t, x=0) = 0 \tag{6}$$

$$G(t, x=0) = 0. (7)$$

Here, the analytical solution Equation (3) contains two terms (T and G) that can be obtained by solving Equations (4-7) once velocity filed u(t,x) and net growth rate $\mu_{net}(t,x)$ are given. By comparing Equation (4) with the water age equations in (Deleersnijder et al., 2001; Shen & Lin, 2006), we can find that T is water age in a one-dimensional system when diffusivity is neglected. It has a unit of time that represents the time elapsed since the water parcel leaves the river head at x=0. On the other hand, G is a non-dimensional number and it represents the accumulative effect of net growth rate during the elapsed time T. If G is larger/smaller than zero,

phytoplankton concentration will increase/decrease. If G is zero, phytoplankton concentration will remain the same. Hereafter, we will call G as accumulative growth.

The combination of T and G disentangles the physical and biological effects in Equation (1) resulting in an elegant expression of phytoplankton concentration in time and space as in Equation (3). Equation (3) is the product of two parts: a(t-T) and e^{a} , both of which have clear physical meanings. a(t-T) relates the phytoplankton concentration at (t,x) to the boundary phytoplankton concentration at a previous time with a time lag of T. Essentially, it states that the water parcel at (t,x) is originated from the upstream boundary (x=0) at time of (t-T). The phytoplankton concentration a(t-T) serves as the initial phytoplankton concentration for the water parcel at (t, x) when it leaves the boundary and travels to the location x. The second part e^{G} tells whether phytoplankton concentration will increase or decrease when phytoplankton reaches its current location at (t, x). It is obtained by integrating the biological effect μ_{net} during the time period from (t-T) to t when phytoplankton is transported downstream. It can be seen from Equation (5) that the accumulative effect depends not only on net growth rate but also on the physical transport. The interpretation of solution actually follows the movement of water parcel from Lagrangian point of view, which becomes more natural if transformation $\frac{d}{dt} = \frac{\partial}{\partial t} + u \frac{\partial}{\partial r}$ is made on the above equations from Eulerian coordinate to Lagrangian coordinate (e.g. Equation 5 is transformed to $\frac{dG}{dt} = \mu_{net}$).

175

176

177

178

179

180

181

182

174

157

158

159

160

161

162

163

164

165

166

167

168

169

170

171

172

173

2.2 Solution with Nonlinear Reaction Term

In Equation (1), we summarize all the biological effects into a single term namely net growth rate μ_{net} . This simplification facilitates our analysis on the coupling between physical and biological processes. It assumes that all the information about the phytoplankton growth and loss can be sufficiently resolved by μ_{net} . However, in reality it is always difficult to estimate an accurate μ_{net} because the acquisition of physical and biological information in time and space is demanding. In addition, there exists nonlinear processes that impact phytoplankton concentration. For

example, zooplankton grazing rate may relate to zooplankton concentration which in turn relates to phytoplankton concentration (Filardo & Dunstan, 1985; Wang & Y.Kuo, 2009). In some cases, phytoplankton self-shading effect can reduce its growth rate under high phytoplankton concentration (Barros et al., 2003). Also, interaction among phytoplankton species may be important under high phytoplankton concentration (Lim et al., 2014). All these factors are difficult to be quantified by the single net growth term. To partially include these effects in the model, we add a feedback mechanism into the μ_{net} in the form of $\mu_{net} = \mu_{net}^0 \cdot (1 + k \cdot C)$ where $\mu_{net}^0(t,x)$ is the initial estimate of net growth rate and k is a constant used to modify μ_{net}^0 depending on phytoplankton concentration C. The modified net growth rate μ_{net} decreases with K is negative/positive and μ_{net}^0 is larger/smaller than zero. With this new form, Equation (1) becomes a partial differential equation with a nonlinear term:

$$\frac{\partial C}{\partial t} + u \frac{\partial C}{\partial x} = \mu_{net}^{0} \cdot (1 + k \cdot C) \cdot C \quad , \text{ for } x \in [0, L].$$
 (8)

The form of Equation (8) is similar to the logistic model that is widely used in biology to describe the population growth of many different kinds of lives on earth such as bacteria (Rice University, 2013). Here, we focus on the feedback mechanism that phytoplankton concentration can affect the net growth rate, especially under high concentration.

On the other hand, the nonlinear term $k \cdot \mu_{net}^0 \cdot C^2$ in Equation (8) plays a similar role as physical mixing in smoothing the spatial gradient of phytoplankton concentration when it has a negative value. The negative nonlinear term means larger attenuation for higher phytoplankton concentrations (large values of C), but smaller attenuation for lower phytoplankton concentrations (small values of C). Along with time, the peaks of phytoplankton concentrations in space will be depressed. It resembles the function of physical mixing that can be important in estuaries (MacCready & Geyer, 2010). This similarity will be further illustrated in Section 4.1.

Although Equation (8) is a nonlinear equation, an analytical solution can still be obtained as:

$$C(t,x) = \frac{a(t-T) \cdot e^G}{1 + k \cdot a(t-T) \cdot (1 - e^G)} \text{, for } x \in [0, L],$$

$$(9)$$

with Equation (5) slightly modified as:

$$\frac{\partial G}{\partial t} + u \frac{\partial G}{\partial x} = \mu_{net}^0 \tag{10}$$

where T remains the same as in Equation (3). Appendix A shows the proof that Equation (9) is the solution to Equation (8).

210

211

2.3 Simple Cases

The exact expressions of the analytical solution Equations (3, 9) depend on the Equations (4-7, 10) given boundary condition, velocity field and net growth rate. In other words, the explicit forms of Equations (3, 9) depend on whether the explicit expressions of T and G are possible. In many cases, explicit forms of the solutions may not be possible if velocity and net growth rate have complicated forms. However, when simplifications are made, we can get explicit solutions.

217

- 2.3.1 Spatially Varying Net Growth Rate and Velocity Field
- When velocity field and net growth rate do not change with time, they can be expressed as u(x) and $\mu_{net}(x)$ or $\mu_{net}^0(x)$. By solving Equations (4-7), we can obtain the form of Equation (3)
 - $T(x) = \int_0^x \frac{d\eta}{u(\eta)}.$ (11)

222

221

as:

$$G(t,x) = \int_0^x \frac{\mu_{net}(\eta)}{u(\eta)} d\eta.$$
 (12)

- With an nonlinear reaction term, we can obtain the expression of Equation (9) with the same T as
- in Equation (11) and

$$G(t,x) = \int_0^x \frac{\mu_{net}^0(\eta)}{u(\eta)} d\eta.$$
 (13)

- 225 2.3.2 Constant Net Growth Rate and Spatially Varying Velocity Field
- Based on 2.3.1, if net growth rate is further regarded as constant, Equations (3, 9) become:

$$C(t,x) = a(t-T) \cdot e^{\mu_{net} \cdot T}. \tag{14}$$

227 and

$$C(t,x) = \frac{a(t-T) \cdot e^{\mu_{net}^0 \cdot T}}{1 + k \cdot a(t-T) \cdot \left(1 - e^{\mu_{net}^0 \cdot T}\right)}.$$
 (15)

where T is the same as in Equation (11).

229 2.3.3 Constant Boundary Condition, Net Growth Rate and Velocity Field

In the simplest case when boundary condition, net growth rate and velocity field do not change with time and space, the solution in Equation (3) is degenerated to:

$$C(x) = a \cdot e^{\mu_{net} \cdot \frac{x}{u}}.$$
 (16)

where a, μ_{net} and u are all constant. Equation (16) is the phytoplankton model presented by Lucas et al. (2009). This means that the phytoplankton model in (Lucas et al., 2009) is a special case of our generic model, which provides a validity for our theory about phytoplankton dynamics.

If there is nonlinear reaction term, Equation (9) becomes:

$$C(x) = \frac{a \cdot e^{\mu_{net}^0 \cdot \frac{x}{u}}}{1 + k \cdot a \cdot \left(1 - e^{\mu_{net}^0 \cdot \frac{x}{u}}\right)}.$$
(17)

236

237

238

239

240

241

242

243

235

2.4 Phytoplankton Prediction in The Downstream

As shown in Equations (3, 9), the phytoplankton concentration in the downstream only depends on the boundary condition once water age and accumulative growth are known, which means that we can use phytoplankton concentration measured at the boundary to predict downstream phytoplankton concentration in time and space.

Based on Equations (3, 9), if we fix at a downstream location $x = x_0$, we can estimate the temporal variation of local phytoplankton concentration:

$$C(t, x_0) = a(t - T(t, x_0)) \cdot e^{G(t, x_0)}$$
(18)

$$C(t,x_0) = \frac{a(t-T(t,x_0)) \cdot e^{G(t,x_0)}}{1+k \cdot a(t-T(t,x_0)) \cdot (1-e^{G(t,x_0)})}$$
(19)

If we fix at a particular time $t = t_0$, we can estimate the spatial distribution of phytoplankton concentration:

$$C(t_0, x) = a(t_0 - T(t_0, x)) \cdot e^{G(t_0, x)}$$
 (20)

247

$$C(t_0, x) = \frac{a(t_0 - T(t_0, x)) \cdot e^{G(t_0, x)}}{1 + k \cdot a(t_0 - T(t_0, x)) \cdot (1 - e^{G(t_0, x)})}$$
(21)

On the other hand, if the spatial distribution of phytoplankton concentration at time $t = t_0$ is known, we can estimate the temporal variation of phytoplankton concentration at the boundary based on Equation (20, 21) as below:

$$C(\xi, x = 0) = b(T^{-1}(t_0 - \xi)) \cdot e^{-G(t_0, T^{-1}(t_0 - \xi))}$$
(22)

251

$$C(\xi, x = 0) = \frac{b(T^{-1}(t_0 - \xi))}{\left[1 + k \cdot b(T^{-1}(t_0 - \xi))\right] \cdot e^{-G(t_0, T^{-1}(t_0 - \xi))} - k \cdot b(T^{-1}(t_0 - \xi))}$$
(23)

where $\xi \in [t_0 - T(t_0, L), t_0], T^{-1}(\xi)$ is the inverse function of $T(t_0, x)$, and b(x) for $x \in [0, L]$

is phytoplankton concentration in space at time $t = t_0$.

254

255

253

3 Results

TFR in many estuaries shares common features in hydrology, geomorphology and water chemistry (Bukaveckas et al., 2011). It often has a regular shape in the longitudinal direction and a constricted cross section under strong fluvial influence, resulting in a transit time changing with river inflow. In addition, the water is usually in abundance of nutrients and suspended particulate matters (Wood et al., 2013). These characterize the interaction between the hydrodynamics and phytoplankton dynamics in TFR as different from other regions in estuaries. Particularly, physical transport may play an important role in regulating phytoplankton distribution (Filardo & Dunstan, 1985; Sellner et al., 1988; Sze, 1981). In this section, we will apply our theory in the TFR of James River by integrating all kinds of available observations.

3.1 Observation in James River TFR

James River is located in the lower Chesapeake Bay. It is about 170 km in length from its fall line to the river mouth (Shen & Lin, 2006). The river inflow can vary from 10 m³/s to over 8000 m³/s with an average river discharge of about 200 m³/s (Fang et al., 1973; U.S. Geological Survey Data, 2018). The James River is characterized by complex hydrodynamics (Shen et al., 1999) and high chlorophyll concentration is often observed (Wood et al., 2013). The tidal influence can propagate up to the Richmod, VA. Generally, the tidal range in the upper James River is about one meter (Shen et al., 2016b), and the tidal current has an amplitude varying from 0.25 m/s to 0.5 m/s. The subtidal current in the upper narrow, deep channels is more influenced by the river flow with speed varying from 0.0 m/s to 3 m/s, while the current speed becomes much smaller in the lower broad expansion. Filardo and Dunstan (1985) conducted a field experiment in the upper James River and found that there is an inverse relationship between river discharge and chlorophyll concentration. Bukaveckas et al. (2011) reported a local chlorophyll-a maximum recurring each summer in the downstream of the confluence of tidal James River and Appomattox River. They pointed out that the chlorophyll-a maximum coincides with low salinity and high turbidity zone, and the location is related to the river geomorphology.

In the TFR of James River, three types of phytoplankton measurements are available on http://web2.vims.edu/vecos/. The first one is continuous monitoring data at fixed stations that

report chlorophyll concentrations every 15 minutes, but there are only a few such stations in James River. The second one is dataflow cruise data showing chlorophyll distribution over a large portion of the river at discrete dates. They have good spatial coverage, but lack temporal resolution. The third one is long-term monthly water quality monitoring data at fixed stations, available from 1985 to the present. The first two types of data are measured as chlorophyll fluorescence, which is different from the chlorophyll-a data of the third type. In the following Section 3.2 and 3.3, we are trying to predict spatial variations in dataflow based on the continuous monitoring data at fixed station. For the comparison, we do not convert chlorophyll fluorescence into chlorophyll-a concentration. Instead, the chlorophyll values at the same location and time are checked to ensure the consistence between the two types of chlorophyll data. In addition, correlation coefficient (CC), and model skill are used to evaluate the comparison between model and observation. The model skill is defined by $SS = 1 - \sum_i (model_i - obs_i)^2 / \sum_i (|model_i - \overline{obs_i}| + |obs_i - \overline{obs_i}|)^2$ (Willmott, 1981), where model, and obs, are time series of modeled and observed chlorophyll,

3.2 Constant Net Growth Rate under Low Flow Condition

and overbar denotes average.

Under low flow conditions when river discharge does not vary considerably, the velocity can be regarded as constant over time. If the net growth rate is also assumed to be constant, the solutions in Equations (14, 15) can be used to estimate downstream phytoplankton concentration based on the boundary condition of phytoplankton concentration.

In the upper James River, chlorophyll concentration in unit of $\mu g/L$ (as a proxy of phytoplankton concentration) is reported every 15 minutes at continuous monitoring Station JMS073.37 (Figure 1a). This serves as the boundary condition of phytoplankton concentration for our model configuration under the assumption that every water parcel passes this station before travelling downstream. The model axis (red line in Figure 1a) starts from JMS073.37 (x = 0) and goes downstream along the river channel. Figure 1b shows the time series of chlorophyll measurements at JMS073.37 for the period 06/01/2008-08/15/2008. Chlorophyll concentration from dataflow data is also available on 08/13/2008 which provides a snapshot of downstream

chlorophyll distribution. The dataflow date are interpolated along the model axis and the result serves as observation data for model comparison.

The river discharge in James River (U.S. Geological Survey Data, 2018) had a small variation during the two months prior to 08/13/2008 when dataflow data of chlorophyll is measured. The average was 37 m³/s with a standard deviation about 16 m³/s. For simplicity, the river discharge is regarded as constant with 37 m³/s, which implies that the velocity field does not change with time. Based on the continuity equation that river discharge (m³/s) equals water velocity (m/s) multiplied by river cross sectional area (m²), we can estimate the velocity filed u(x) along the river. Note that the effect of tidal excursion is neglected in the calculation as we focus on the long-term chlorophyll variation here and the residual velocity sufficiently serves the purpose. The estimated velocity field along with the river cross sectional area are shown in Figure 2 based on the 10-meter resolution bathymetry data from Federal Emergency Management Agency (2010).

Given the phytoplankton boundary condition at JMS073.37 and velocity field, Equation (14) can be implemented in the TFR of James River. By using constant net growth rates, downstream phytoplankton can be estimated in unit of µg[Chl]/L. These net growth rates are based on Qin and Shen (2017), but are modified to best estimate downstream chlorophyll concentration. Figure 3a is based on Equation (14) using net growth rates of -0.028 day⁻¹. The modeled chlorophyll generally matches the observation. The decreasing trend of chlorophyll from upstream to downstream is well reproduced. However, there are three chlorophyll peaks that largely deviate from the observation occurring at locations: around 5 km, 10 km and 12 km. These spatial peaks are resulting from the temporal oscillations of boundary chlorophyll concentration at times: around August 5th, July 25th and July 20th (Figure 1b). Because physical mixing is not included in Equation (14), these boundary oscillations are advected to the downstream as chlorophyll peaks in space. The missing of these peaks in observational data shows that physical mixing is also important in the TFR of James River as shown by Li et al. (2004). Additionally, if we applied a small trial net growth rate of -0.01 day⁻¹ in the model, it over-predicts the chlorophyll distribution (Figure 3a) and the result merely represents the advection the boundary condition toward the downstream. If we applied a larger value -0.05 day⁻¹, the chlorophyll concentration in the downstream is overly attenuated except the large peaks. Overall, the mean net growth rate for phytoplankton in July-August, 2008 is about -0.03 day⁻¹ and this magnitude is consistent with the results in Qin and Shen (2017). The negative value suggests that a chlorophyll maximum may be located in the upstream of Station JMS073.37 as shown in Figure 1a. Also, we noticed that the two different chlorophyll observations (dataflow data and continuous monitoring data) used for comparison are consistent regarding the chlorophyll concentration at (t = 08/13/2008, x = 0) which is around 25 µg/L (Figure 3).

Figure 3b shows chlorophyll estimates with nonlinear term. The results are based on Equation (15) with two sets of parameters: $(\mu_{net}^0 = -0.015 \text{ day}^{-1}, k = 0.05 \text{ µg}^{-1} \cdot \text{L})$ and $(\mu_{net}^0 = -0.0075 \text{ day}^{-1}, k = 0.2 \text{ µg}^{-1} \cdot \text{L})$. Compared to the results in Figure 3a, the model skill in chlorophyll is improved as the estimates match observation better visually with less chlorophyll oscillation and depressed peaks along the river. This is attributed to the negative nonlinear term contained in Equation (8) that larger decay rate is associated with higher chlorophyll concentration. Given that chlorophyll concentration varies around [20, 60] µg/L, the apparent net growth rate $\mu_{net} = \mu_{net}^0 \cdot (1 + k \cdot C)$ varies about [-0.06, -0.03] day⁻¹ and [-0.0975, -0.0375] day⁻¹ for the two different sets of parameters respectively. Therefore, a large k in Equation (8) means that the net growth rate has a large variation by relating to phytoplankton concentration.

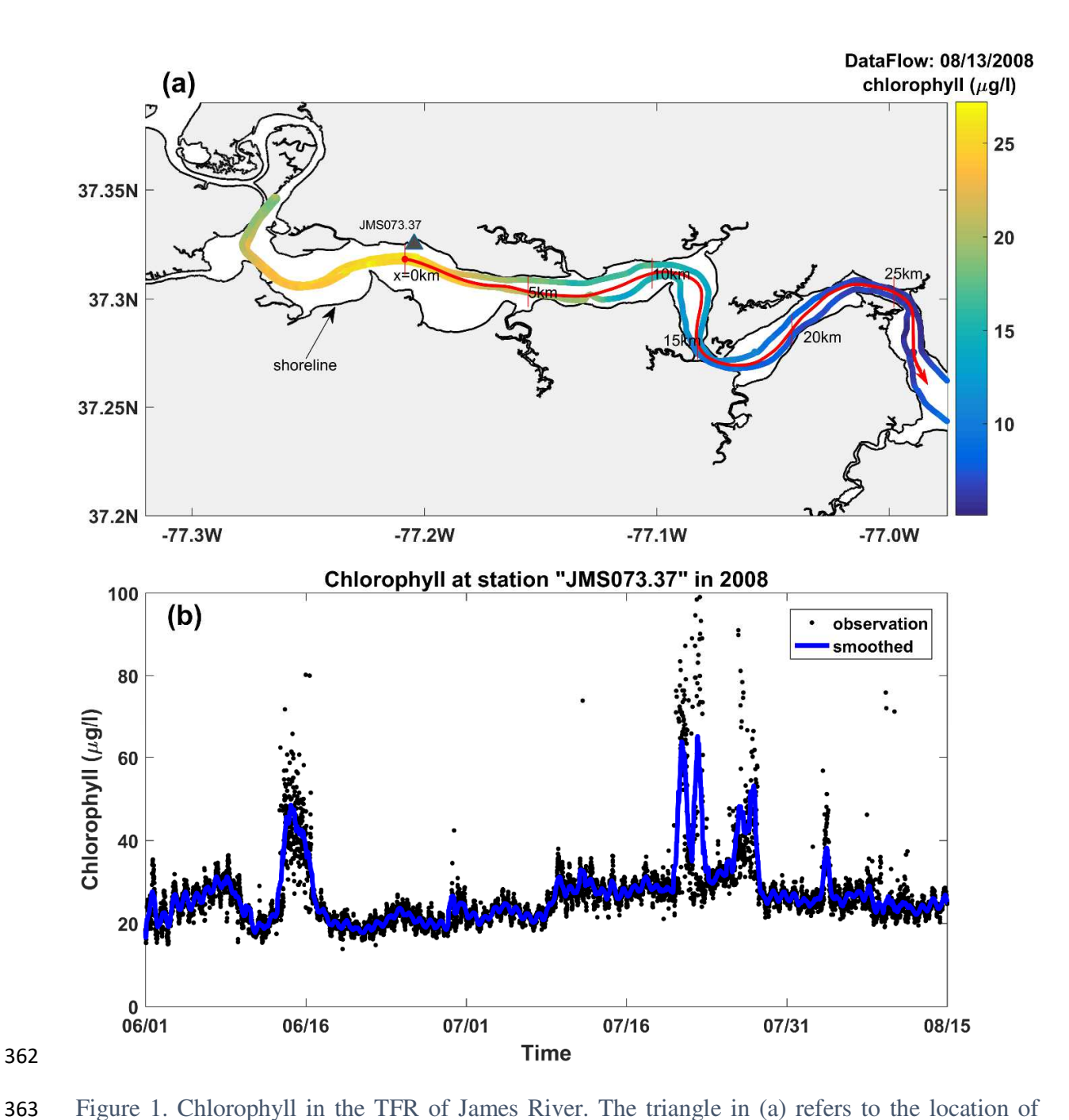


Figure 1. Chlorophyll in the TFR of James River. The triangle in (a) refers to the location of continuous monitoring Station JMS073.37 and chlorophyll time series from 06/01/2008 to 08/15/2008 is shown in (b) with moving average in blue line using 12-hour window. The color lines in (a) represent chlorophyll distribution from dataflow measurement on 08/13/2008 in the upper James River. The red line in (a) shows model axis starting from Station JMS073.37.



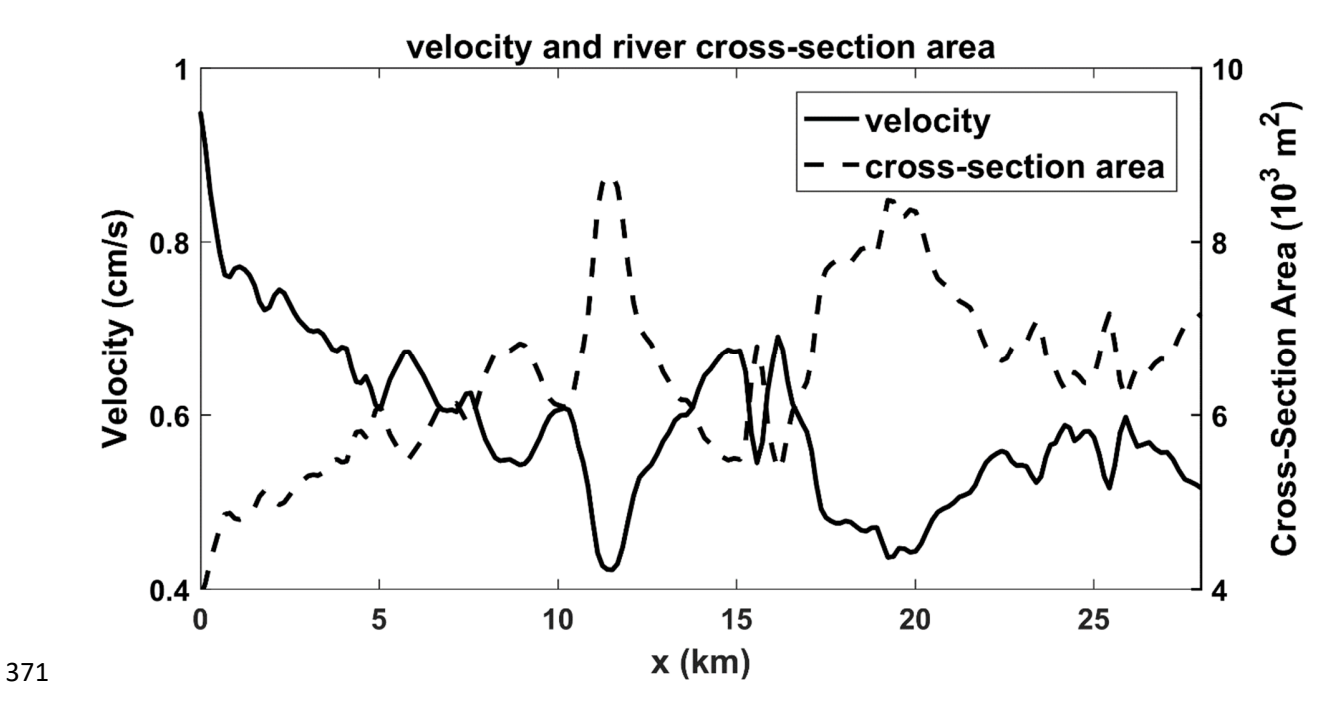


Figure 2. Average velocity along James River in the TFR and the river cross-section area. The constant river discharge 37 m³/s is assumed for the calculation under low flow condition.

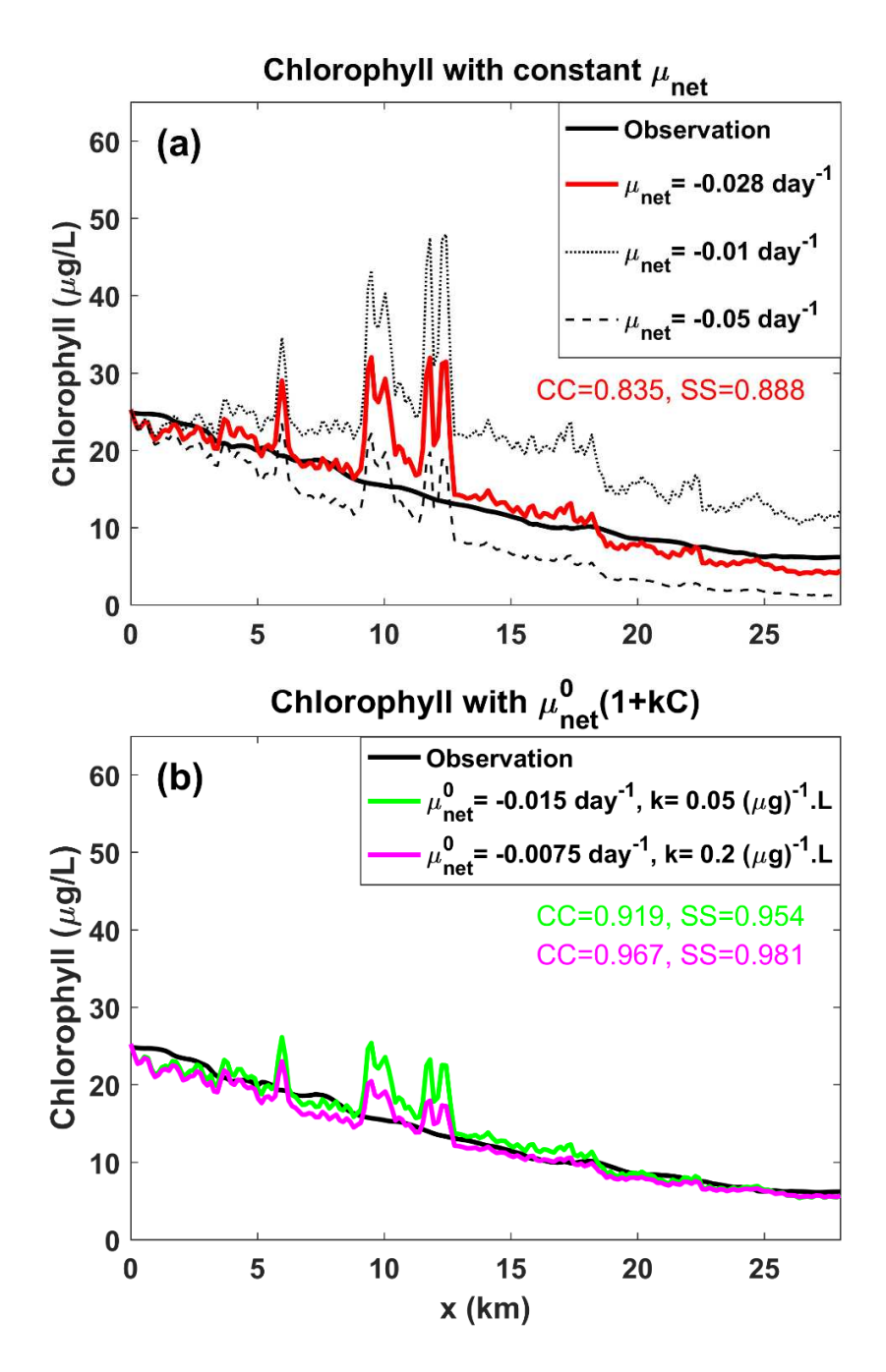


Figure 3. Chlorophyll estimates on 08/13/2008 with constant net growth rates under low flow condition. The x-axis starts from Station JMS073.37 along the river. The upper panel shows model result with net growth rate -0.028 day⁻¹ that is chosen because it best predict downstream chlorophyll variation. Two other modeling results with a smaller net negative growth rate -0.01 day⁻¹ (dotted line) and a larger negative net growth rate -0.05 day-1 (dashed line) are shown for comparison. The lower panel shows model results with two sets of trial parameters:

 $(\mu_{net}^0 = -0.015 \text{ day}^{-1}, k = 0.05 \text{ } \mu\text{g}^{-1} \cdot \text{L})$ and $(\mu_{net}^0 = -0.0075 \text{ day}^{-1}, k = 0.2 \text{ } \mu\text{g}^{-1} \cdot \text{L})$ based on based on Equation (15). The chlorophyll observation (black line) is interpolated from dataflow data on 08/13/2008 as shown in Figure 1.

3.3 Constant Net Growth Rate Under High Flow Condition

To test whether Equation (14, 15) can still work under high flow condition, we choose a period 07/01/2006-07/06/2006 during which the river discharge changed from below $200 \text{ m}^3/\text{s}$ to over $2000 \text{ m}^3/\text{s}$. The mean river discharge was about $435 \text{ m}^3/\text{s}$ with a standard deviation of about $452 \text{ m}^3/\text{s}$. In order to apply Equation (14, 15) in the TFR of James River, the flow rate is still regarded as a constant of $435 \text{ m}^3/\text{s}$ although it is highly variable. Similar to Figure 2, the velocity field along the river channel is calculated (not shown) in an inverse relationship to the river cross-sectional area. In addition, chlorophyll dataflow data is available on 07/06/2006 as shown in Figure 4a. Because of the large river flow, the retention time of water parcel in our computation domain is short (less than one week), which means that downstream chlorophyll distribution on 07/06/2006 is only related to boundary condition in the prior week. Figure 4b shows the chlorophyll time series from continuous monitoring data at Station JMS073.37, which serve as the chlorophyll boundary condition at x = 0.

Similar to Figure 3, Figure 5a-b show model results based on Equation (14, 15). Figure 5a is obtained with constant net growth rate of -0.4 day⁻¹. Most of the chlorophyll estimate is overestimated especially during the range $x \in [0, 10]$ km. Figure 5b is obtained with the net growth rates modified to approximate biological feedback mechanism or physical mixing; and two sets of parameters are used: $(\mu_{net}^0 = -0.3 \text{ day}^{-1}, k = 0.05 \text{ µg}^{-1} \cdot \text{L})$ and $(\mu_{net}^0 = -0.15 \text{ day}^{-1}, k = 0.2 \text{ µg}^{-1} \cdot \text{L})$. Compared to Figure 5a, the chlorophyll estimates in Figure 5b are improved as the estimates are closer the observation visually between $x \in [10, 25]$ km and the chlorophyll oscillations inherited from the continuous monitoring data are largely depressed. However, the modeled chlorophyll in $x \in [0, 10]$ is still much higher than the observation. One cause for the overestimation is the mismatch of chlorophyll measurements between continuous monitoring data

and dataflow data as indicated by the chlorophyll concentrations at (t = 07/06/2006, x = 0) where the values are around 18 µg/L and 10 µg/L respectively (Figure 5b). The reason for the mismatch is likely because the continuous monitoring Station JMS073.37 is located nearshore, while the passage of dataflow cruise is along the river channel.

409

410

411412

413

414

415

416 417

418

419

420

421

422

423

424 425

426

427

428

429

430

431432

433

434

435

436 437

In order to reduce the mismatch between different chlorophyll measurements, the continuous monitoring chlorophyll during 07/01/2006-07/06/2006 is scaled by multiplying a factor of 0.55 to be new boundary condition (indicated in Figure 5c). This ensures that two types of data are consistent. The resulting chlorophyll estimates based on Equation (14, 15) are shown in Figure 5c-d. Overall, the results are further improved with respect to Figure 5a-b. In Figure 5c, the chlorophyll estimate is for a constant net growth rate of $\mu_{net} = -0.2 \text{ day}^{-1}$, which represents the average net growth rate in the downstream. Figure 5d shows the results for net growth rates with nonlinear reaction term with two sets of parameters: $(\mu_{net}^0 = -0.2 \text{ day}^{-1}, k = 0.05 \text{ } \mu\text{g}^{-1} \cdot \text{L})$ and $(\mu_{net}^0 = -0.1 \text{ day}^{-1}, k = 0.2 \text{ } \mu\text{g}^{-1} \cdot \text{L})$. If the modified chlorophyll at the boundary is around [10,20] μg/L (multiplying the observational values in Figure 4b by 0.55), the two sets of parameters translate to net growth rates: [-0.3, -0.4] day⁻¹ and [-0.3, -0.5] day⁻¹ respectively. The chlorophyll estimates in Figure 5c-d are generally similar, but with smaller chlorophyll peaks in Figure 5d because nonlinear term in Equation (8) has a similar effect as physical mixing in smooth horizontal peaks (see discussion in Section 4.1). The two model results all reproduce the general trend of observational chlorophyll in the downstream in that chlorophyll stays high (around 10 µg/L) in $x \in [0, 10]$ km; drops rapidly in $x \in [10, 15]$ km; and stays low (around 5 µg/L) in $x \in [15, 25]$ km. Compared to the results in Figure 3b under low flow condition, both the observation and model estimate in Figure 5c-d present more chlorophyll oscillation in downstream. This is probably due to the short transit time under high flow condition, so that chlorophyll oscillation from the boundary is still preserved instead of being completely smoothed by physical mixing. The mismatch between the phases of chlorophyll oscillation is because of the simplified velocity filed resulting from the assumption of a constant flow rate. Nevertheless, the results show that our model still can predict the general tread of chlorophyll distribution in the downstream under high flow condition although improvement may be achieved by using a varying velocity field.

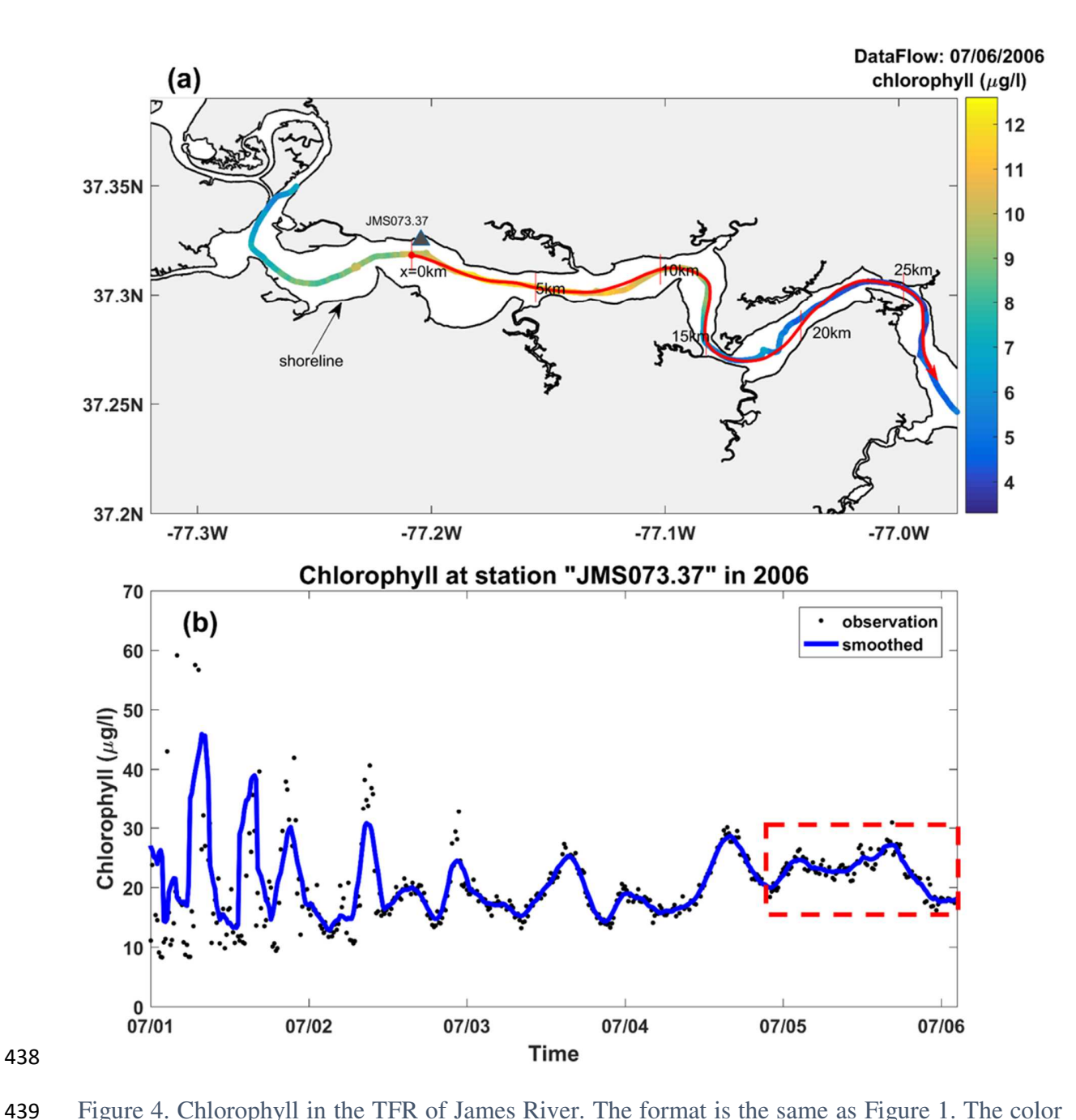


Figure 4. Chlorophyll in the TFR of James River. The format is the same as Figure 1. The color lines in upper panel (a) represent chlorophyll distribution from dataflow measurement on 07/06/2007 in the upper James River. The lower panel (b) shows chlorophyll time series at Station JMS073.37 from 07/01/2006 to 07/06/2006 with moving average in blue line using 12-hour window.

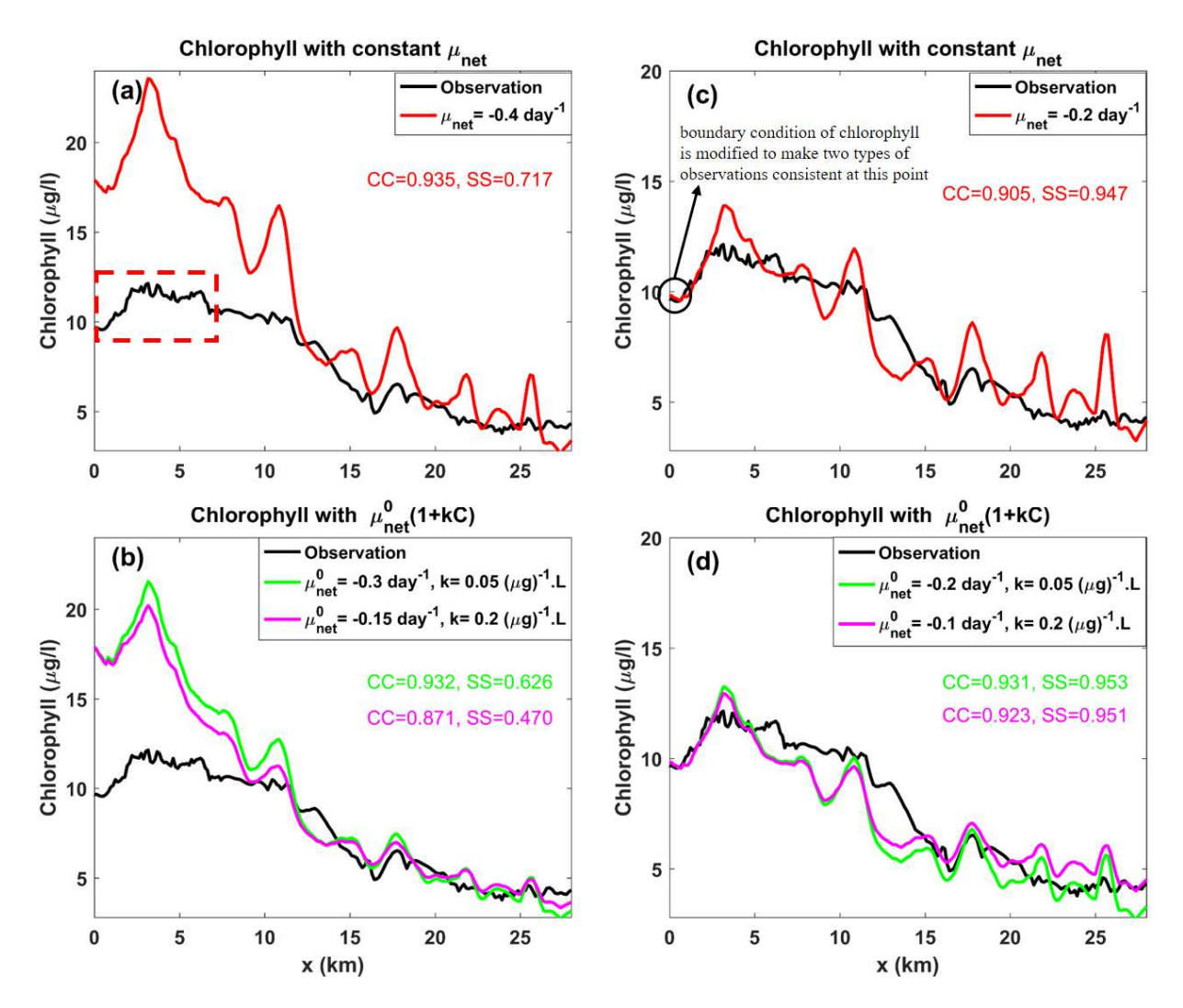


Figure 5. Chlorophyll estimates on 07/06/2006 with constant net growth rates under high flow condition. The upper left panel (a) shows model result with net growth rate of $-0.4 \, \text{day}^{-1}$ based on Equation (14). The lower left panel (b) shows model results for two sets of trial parameters: $(\mu_{net}^0 = -0.3 \, \text{day}^{-1}, k = 0.05 \, \mu \text{g}^{-1} \cdot \text{L})$ and $(\mu_{net}^0 = -0.15 \, \text{day}^{-1}, k = 0.2 \, \mu \text{g}^{-1} \cdot \text{L})$ based on Equation (15). Note that there is a mismatch for chlorophyll measurements between the continuous monitoring data and dataflow data at (t=07/06/2006, x=0). Panels (c, d) are similar to panels (a, b), but are obtained with modified continuously monitoring data by a factor of 0.55. The panel (c) is for constant net growth rate of $-0.2 \, \text{day}^{-1}$, while the parameters for the results in panel (d) are $(\mu_{net}^0 = -0.2 \, \text{day}^{-1}, k = 0.05 \, \mu \text{g}^{-1} \cdot \text{L})$ and $(\mu_{net}^0 = -0.1 \, \text{day}^{-1}, k = 0.2 \, \mu \text{g}^{-1} \cdot \text{L})$. The net growth rates in (a) and (c) are chosen based on Qin and Shen (2017) to best predict downstream chlorophyll variations. The chlorophyll observation (black line) is interpolated from dataflow data

on 07/06/2006 as shown in Figure 4. The observational data marked in the box in (a) with dash line roughly correspond to the continuously monitoring chlorophyll data marked in the box in Figure 4b.

460

461

462

463

464

465

466

467

468

469

470

471

472

473

474

475

476

477

478

479

480

481

482

457

458

459

3.4 Variable Net Growth Rate and Velocity Field

In this section, we apply Equations (3, 9) in the TFR of James River with spatiotemporally varying net growth rate and velocity field. Figure 6 shows the model domain that starts from Station TF5.2A. There are 5 long-term water quality stations from Chesapeake Bay Program (2016): TF5.2A, TF5.2, TF5.5, TF5.5A, and TF5.6 providing measurements for NO₃, NH₄, PO₄, water temperature and light attenuation coefficient. Here, we interpolate the measurement data in time and space to estimate the phytoplankton net growth rate μ_{net}^0 in the TFR of James River and the detail of the calculation is attached in Appendix B. Formulations of water quality models (Cerco & Noel, 2004; Park et al., 1995) are used to computer μ_{net}^0 by integrating environmental factors. The simulation period is selected to be 1999-2005 when different hydrological conditions are included (Figure C1). Figure 7 shows the μ_{net}^0 from 1999 to 2005 at 4 water quality monitoring stations below TF5.2A at noon time when μ_{net}^0 is maximum during the daytime. On the other hand, the nighttime μ_{net}^0 becomes negative (not shown) because photosynthesis is shut down, but phytoplankton metabolism and predation by higher trophic levels are not. μ_{net}^0 has a larger magnitude at Station TF5.3 than at other stations probably because of the better light condition in the upper James River around Station TF5.3, as indicated by the distribution of light attenuation in Figure B1. The variations of μ_{net}^0 at downstream Stations TF5.5, TF5.5A and TF5.6 share similar features due to

peak and a fall peak, and has a trough in the winter. In the summer months, μ_{net}^0 varies much

the similar geomorphology at these stations where river channel is broad and shallow, which is

different from TF5.3. Also, μ_{net}^0 presents strong seasonal variabilities. Normally, it has a spring

Because velocity observation in this region is limited, we obtain velocity field from numerical model of SCHISM that was applied in the entire Chesapeake Bay (Ye et al., 2018; Zhang & Baptista, 2008; Zhang et al., 2016). The velocity is tidal-averaged over the river cross section resulting in a one-dimensional velocity filed u(t,x) in the TFR of James River. Based on Equations (4, 6), we further calculated the water age from 1999 to 2005 in the model domain starting from Station TF5.2A. Figure 8 shows the time series of water age at 4 downstream stations below TF5.2A. The water age increases as it goes downstream and has strong interannual variability that is generally larger in 1999, 2001, 2002, but smaller in 2003 and 2004. Similarly, based on Equations (7, 10), we calculated the accumulative growth and Figure 9 shows the results at the same 4 stations as in Figure 8. The accumulative growth represents the accumulated biological effect and the positive values mean that the phytoplankton biomass will increase as it moves downstream after leaving the boundary at TF5.2A. The accumulative growth has a smaller magnitude at station TF5.3, while it is larger at stations TF5.5, TF5.5A and TF5.6. All the 4 stations share similar interannual variabilities for accumulative growth with higher values from 1999 to 2002 and smaller values in 2003 and 2004.

With the water age and accumulative growth known for the TFR of James River, we can evaluate the analytical solutions of Equations (3, 9) with the boundary condition of chlorophyll-a measured at TF5.2A. Figure 10 shows the results against observational data. Both solutions well reproduce the seasonal variability of chlorophyll-a that it is normally small in the winter and peaks during the summer months. Also, the interannual variability is well captured (e.g. higher chlorophyll-a concentrations in 1999-2002 and 2005, and smaller chlorophyll-a concentrations in 2003 and 2004). However, the solution based on Equation (3) presents many chlorophyll-a peaks. Although these peaks generally correspond to the high chlorophyll-a data, they are much higher than the observations. The cause is related to the form of the Equation (1) of phytoplankton dynamics that allows phytoplankton to grow exponentially and unlimited as long as it has a positive net growth rate. With an nonlinear reaction term, the result from Equation (9) is more reasonable and the high chlorophyll-a peaks are depressed. Additionally, we notice that the difference between the two solutions only happens under high chlorophyll-a concentration when strong feedback effect is associated with Equation (9). Overall, the analytical model can well predict the downstream chlorophyll-a regarding the seasonal and interannual variations. The error

mainly results from the insufficient temporal and spatial resolutions of long-term monitoring data (Figure C1), and insufficient representation of the physical mixing by the nonlinear term.

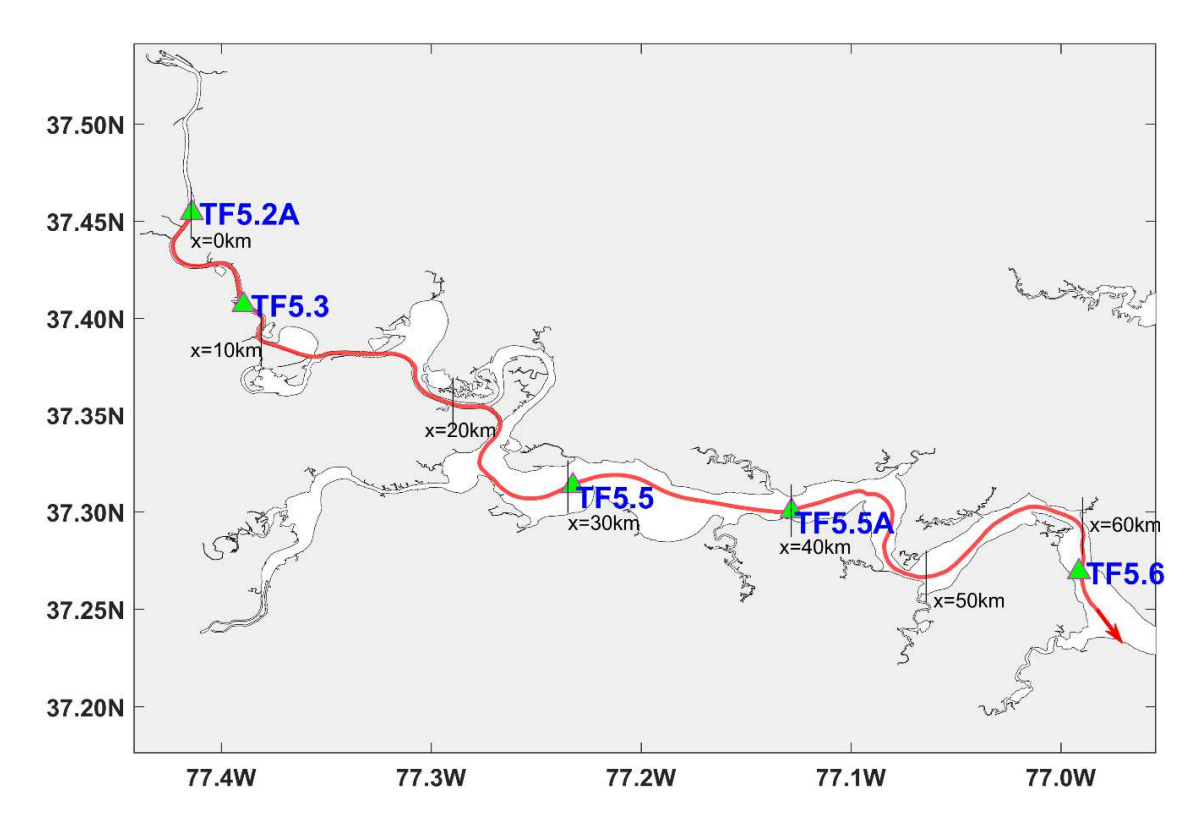


Figure 6. The TFR of James river with 5 long-term monitoring stations (triangles): TF5.2A, TF5.3, TF5.5, TF5.5A and TF5.6. The red line is our model axis starting from Station TF5.2A.

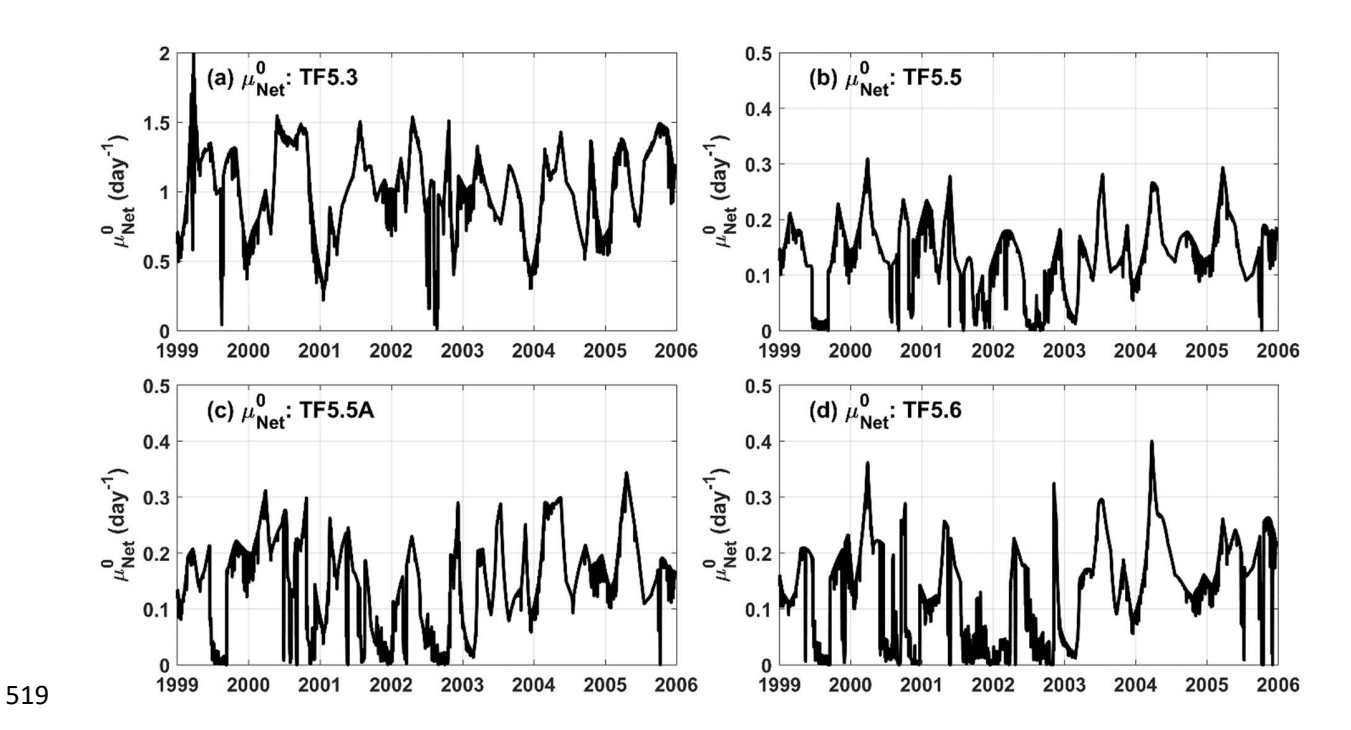


Figure 7. Phytoplankton net growth rates at noon time at 4 water quality monitoring stations.

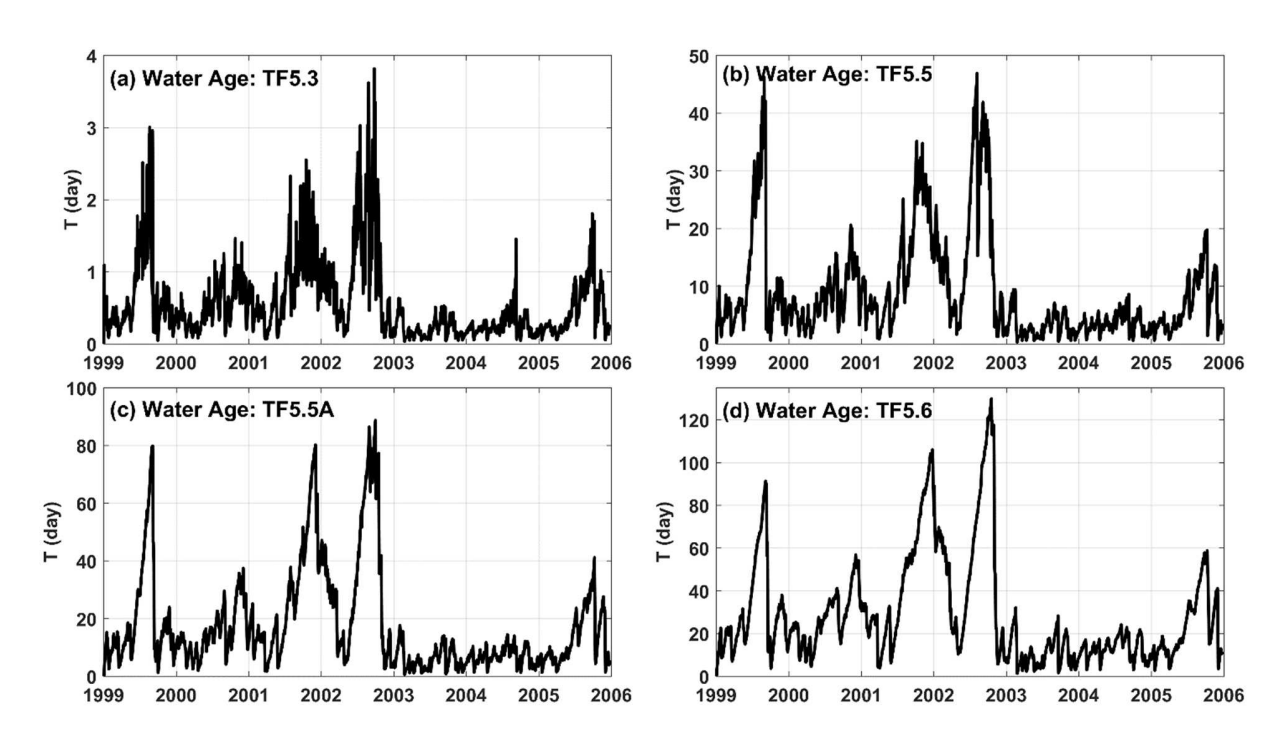


Figure 8. Time series of water age T(t,x) at 4 water quality monitoring stations in the upper James River from 1999 to 2005. The water age is defined as the elapsed time since a water parcel leaves TF5.2A.

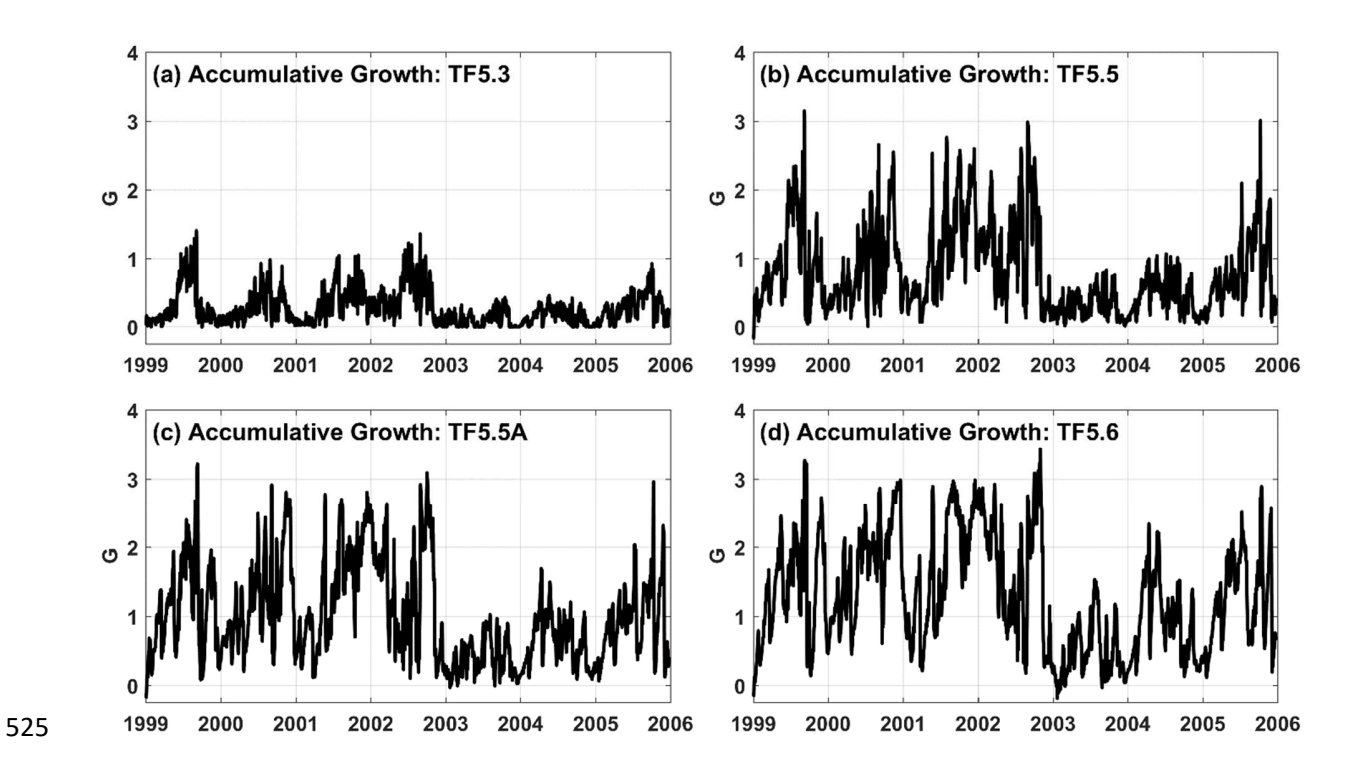


Figure 9. Time series of accumulative growth G(t,x) at 4 water quality monitoring stations in the upper James River from 1999 to 2005.

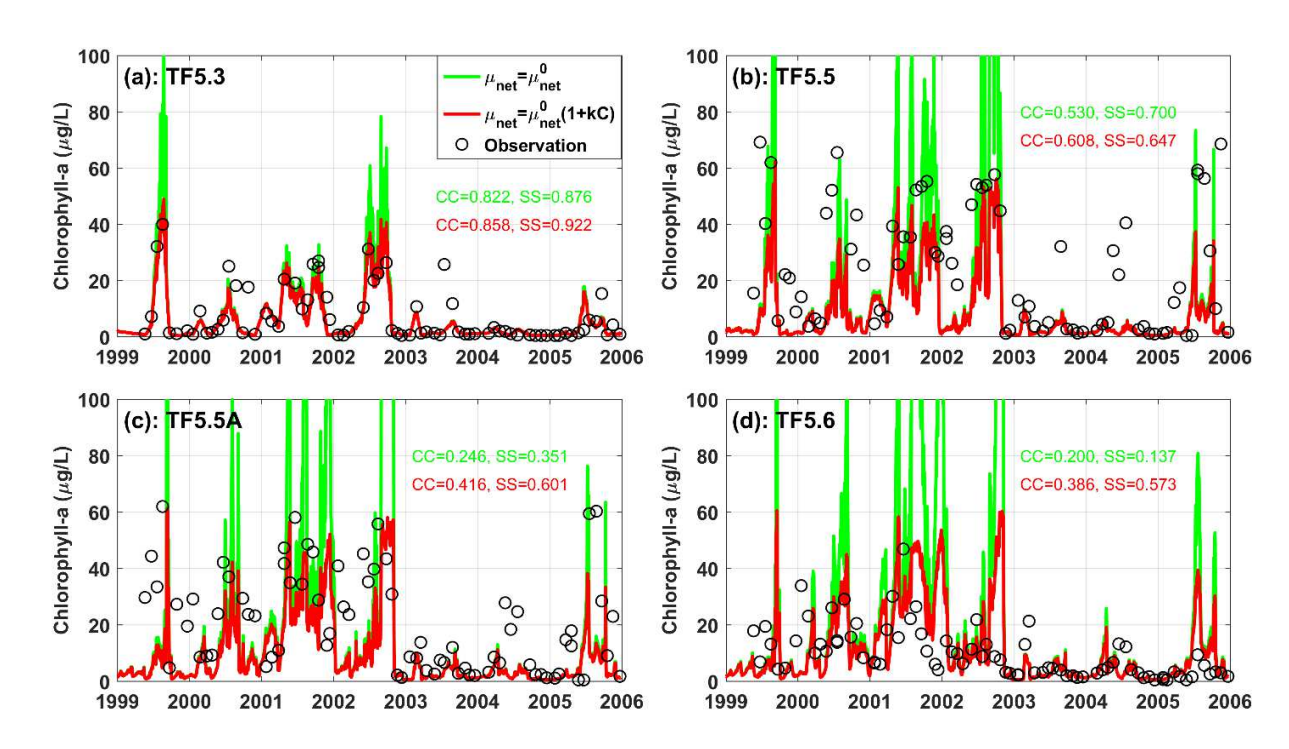


Figure 10. Time series of chlorophyll-a from the analytical model at 4 stations in the upper James River. The modeled chlorophyll-a are compared with long-term monitoring data (circles) from Chesapeake Bay Program. The green lines are the results based on Equations (3), while the red lines are results with an nonlinear reaction term based on Equation (9) with $k = -0.015 \, (\mu g)^{-1} \cdot L$.

4 Discussion

536

537

538

539

540541

542

543

544

545546

547

548549

550

551

552

553554

555

556

557

558

559

560

561

562

563

564

4.1 Analysis on the Model Results

Water age is the elapsed time after phytoplankton leaves its origin. It represents the time that allows phytoplankton to grow or decay during its transport from upstream to downstream. The accumulative growth is the accumulation of biological effects in time from upstream to downstream. It is a non-dimensional number that represents how phytoplankton biomass changes relatively to its original concentration at the starting points. If it is larger/smaller than zero, the biomass concentration will increase/decrease; while if it is zero, the biomass concentration will keep unchanged. The fact that the accumulative growth is determined by phytoplankton net growth rate and the time phytoplankton being transported is important for us to understand phytoplankton variation in time and space. For example, if a high phytoplankton concentration is observed at one particular location, it could be attributed to the accumulation of biological growth resulting in a large accumulative growth or the high phytoplankton concentration advected from upstream. Further, if the high phytoplankton centration is related to the large accumulative growth, it could be due to large net growth rate or long transit time (large water age). When transit time is fixed, larger net growth rate means that phytoplankton can grow faster resulting in higher phytoplankton concentration. In contrast, when net growth rate is fixed, longer transit time allows phytoplankton to grow for a longer time, which can also result in higher phytoplankton concentration. Therefore, physical and biological processes are tightly coupled in determining the phytoplankton concentration regarding its temporal variation and spatial distribution.

In the analytical model, local sources like phytoplankton from benthic resuspension are not considered. It is assumed that all phytoplankton seeds originate from the upstream, which makes the boundary condition important as shown in the form of Equation (3). The variation of boundary phytoplankton concentration such as chlorophyll peaks influences the downstream phytoplankton concentrations. This can be seen by comparing the continuous monitoring chlorophyll data (marked in the box) in Figure 4b with the dataflow chlorophyll data (marked in the box) in Figure 5a (note earlier date corresponds to further downstream location). However, this does not mean that boundary condition completely determines the downstream phytoplankton because physical transport and biological factors are also important. In the regions of long residence time,

phytoplankton have enough growth time to reach its maximum concentration that is ultimately limited by the local environmental resources regardless of the initial condition.

565

566

567

568

569570

571

572

573

574575

576

577

578

579580

581 582

583

584

585

586

587

588

589

590

591

592

593 594 For the solutions of phytoplankton concentration in Equations (3, 9), their expressions depend on the forms of water age and accumulative growth. In many cases, explicit expressions of the solutions maybe not possible if the velocity filed and phytoplankton net growth rate have complicated forms. For some simple cases, we can get the explicit expressions for phytoplankton concentration as shown in 2.3. In the simplest situation when velocity, net growth rate and boundary condition are all constant, the solution in Equation (3) is degenerated to the solution for a steady and uniform system that is discussed by Lucas et al. (2009). However, our solutions in Equations (3, 9) are more generic, which describes the evolvement of phytoplankton concentration in a variables system with time and space.

The successful application of the analytical model in the TFR of James River proves the validity of the model in capturing the key elements in regulating phytoplankton growth. In James River, traditional numerical models or empirical models are capable of simulating the long-term variations of chlorophyll on seasonal or interannual timescales, and their results are usually evaluated against monthly observational data (Chesapeake Environmental Communications, 2015; Fitzpatrick et al., 2014; Shen et al., 2017). However, these models are lacking of the capability to reproduce chlorophyll results on fine scales. In this study, our analytical solution can be used to reproduce short-term variabilities of fine-resolution chlorophyll, and the results are compared with fine-resolution dataflow chlorophyll. For the long-term simulation (low-resolution), our modeled chlorophyll in Figure 10 has similar model skill compared to previous model. In Figure 3 and Figure 5, simplified solutions with constant net growth rates are used to predict downstream chlorophyll distribution under low and high flow conditions. Different rates lead to different results that could overestimate or underestimate the downstream chlorophyll concentration. For the two cases in our study, the net growth rate is about -0.03 day⁻¹ (Figure 3a) under low flow condition, while it is about -0.2 day⁻¹ (Figure 5c) under high flow condition. In addition, the results in Figure 3b and Figure 5d with feedback mechanism match the results visually better than the ones in Figure 3a and Figure 5c, although both solutions can reproduce the general distribution of downstream chlorophyll distribution. For the more general case, Figure 10 shows the results with variable velocity field and net growth rate. Although the boundary condition is based on the monthly chlorophyll-a data at TF5.2A and the phytoplankton net growth rate is also inferred from the monthly water quality measurements only available at 5 stations, the predicted chlorophyll-a matches the observational chlorophyll-a well regarding the seasonal and interannual variations. For both model results and observational data, the chlorophyll-a is generally smaller in winter and higher in summer with oscillations. In addition, for all the 4 stations in Figure 10, 2003 and 2004 are two exceptional years in that the chlorophyll-a concentrations are small compared to other years. Consistent with the results in Figure 3b and Figure 5d, the solution with feedback mechanism in Figure 10 performs better. The major improvement is that many chlorophyll-a peaks are depressed thanks to the nonlinear term in Equation (8).

Mathematically, the nonlinear term $k \cdot \mu_{net}^0 \cdot C^2$ has a similar effect as physical mixing in depressing the peaks when it has a negative value, which is illustrated in Figure 11. The nonlinear term reduces concentrations of the chlorophyll-a peaks, but keeps lower chlorophyll-a concentrations nearly unchanged. The difference for physical mixing is that it not only reduces the peak values, but also increases the chlorophyll-a concentration in the lower part at the same time. Because there are many uncertainties in estimating the net growth rate and velocity field, it is acceptable to approximate the physical mixing effect in our model using a nonlinear reaction term $\mu_{net}^0 \cdot (1 + k \cdot C) \cdot C$. This alternative form of phytoplankton growth term provides more flexibility to mimic physical mixing effect with the combination of $\mu_{\scriptscriptstyle net}^{\scriptscriptstyle 0}$ and k . Different from physical mixing, the sink term $k \cdot \mu_{net}^0 \cdot C^2$ can reduce phytoplankton concentration at non-peak regions, while physical mixing tends to enhance the concentration. To compensate this, we can adjust the $\mu_{\scriptscriptstyle net}^{\scriptscriptstyle 0}$ to increase the phytoplankton concentration at non-peak regions. Though this method is not physically based, it provides a way to simulate mixing effect on phytoplankton distribution in our analytical model, and yields an analytical solution. In Equation (8), the effect of physical mixing is not separable from the biological effect from the negative feedback mechanism. However, when phytoplankton concentration is low when the feedback mechanism can be neglected (Barros et al., 2003; Rice University, 2013), we can largely attribute the nonlinear effect to the physical mixing.

Figure 10 shows the strong interannual variability of chlorophyll-a in TFR of James River. Besides the influence of boundary condition, the interannual variability of chlorophyll-a for the 4 stations in Figure 10 is also attributed to the accumulation of biological processes. This is shown

by the accumulative growth in Figure 9 that shares a similar interannual variation as chlorophylla in Figure 10. Because there is no strong interannual variation for phytoplankton net growth rate (Figure 7), the interannual variation of accumulative growth is in turn largely related to water age (Figure 8), which is controlled by river flow. The correlation between river flow and water age is shown in Figure 12. The correlation is most obvious at Station TF5.3 and goes down visually towards downstream. In 2003 and 2004, the river flow is relatively high with maximum flow rate over 1600 m³/s (Figure C1). The annual mean flow rates are 413.6 m³/s and 269.2 m³/s for 2003 and 2004 respectively, while the annual mean flow rates from 1999 to 2002 are all below 140 m³/s. Therefore, the interannual variation of James River flow is responsible for the interannual variation of water age with an inverse relationship as high flow causes short transit time. Based on these analyses, the interannual variation of James River flow is one cause for the interannual variation of chlorophyll-a in the TFR of James River.

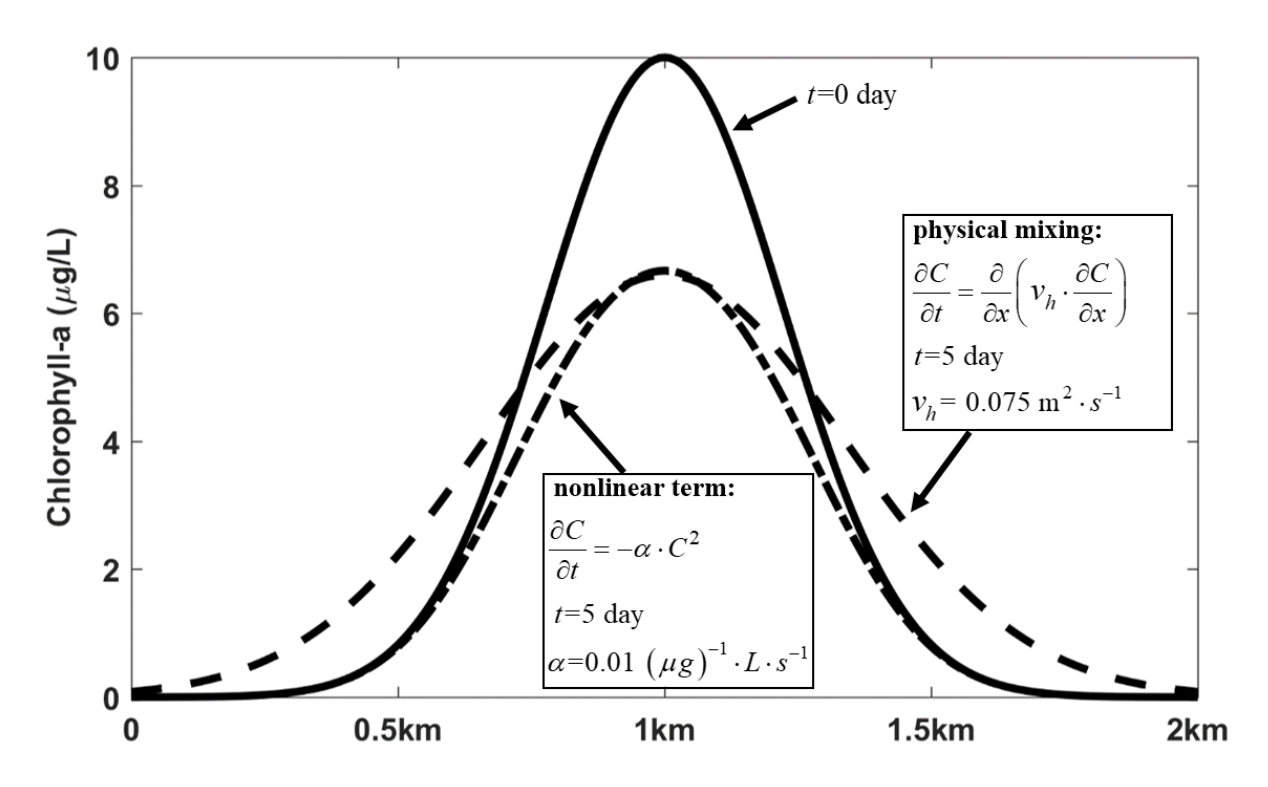


Figure 11. The evolvement of chlorophyll-a distribution with time, which has a Gaussian shape (solid line) at the beginning. The dash line represents the chlorophyll-a distribution with physical mixing after 5 days, while the dash-dotted line represents the chlorophyll-a distribution with nonlinear term after 5 days.

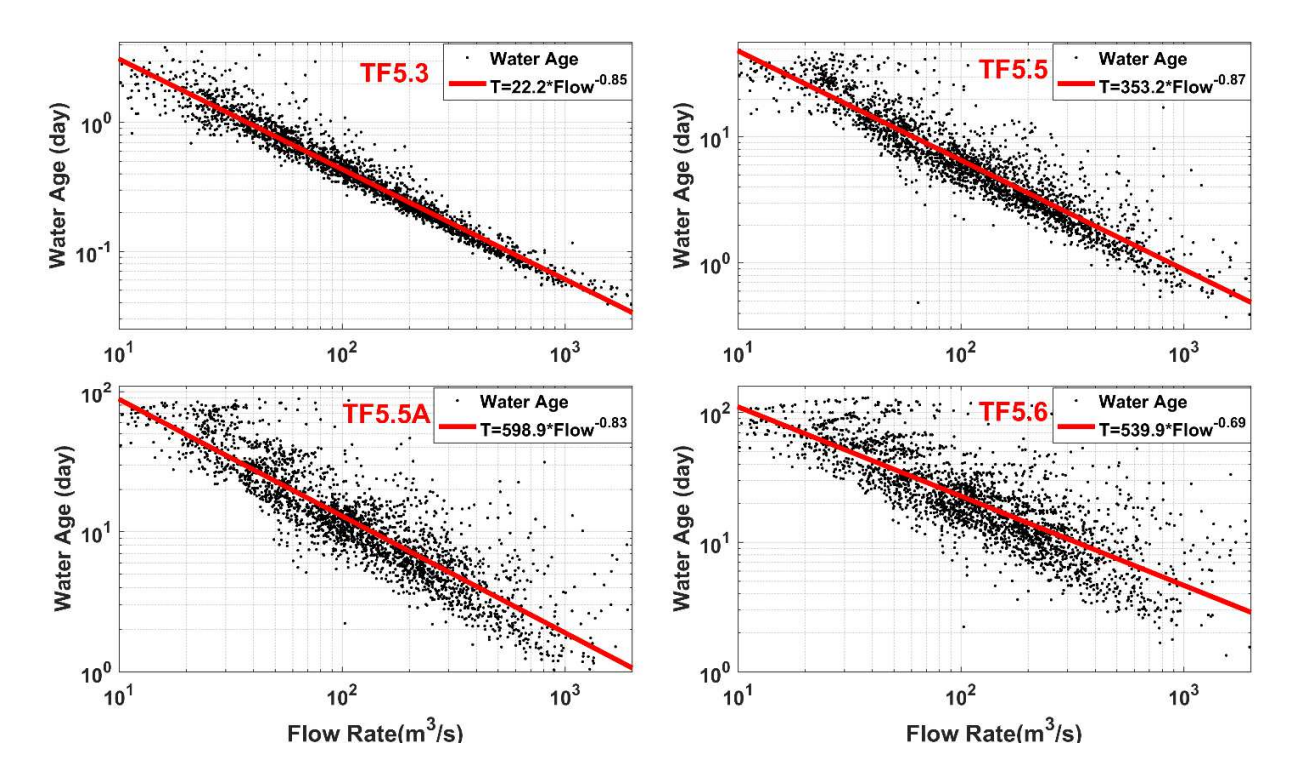


Figure 12. Water age versus James River flow rate at 4 stations in the TFR of James River.

4.2 Local Chlorophyll-a Maximum in TFR

LCM refers to the region in TFR with elevated chlorophyll-a concentration (Bukaveckas et al., 2011). It could be related to changes of river geomorphology or biological factors such as light condition (Bukaveckas et al., 2011; Pennock, 1985). The high primary production in this region can impact the food webs and local ecosystem (Cloern, 2006). Here, we study it by using our analytical solutions. By assuming that boundary condition, velocity field and net growth rate do not change with time, we can get the downstream chlorophyll-a distribution according to Equations (11, 12):

$$C(x) = a \cdot e^{\int_0^x \frac{\mu_{net}(\eta)}{u(\eta)} d\eta}, \qquad (24)$$

where a is the constant boundary condition. Since the necessary condition for chlorophyll-a to get maximum in space is $\frac{\partial C}{\partial x} = 0$, Equation (24) leads to

$$\mu_{net}\left(x_{m}\right) = 0, \tag{25}$$

where x_m is the location for $\frac{\partial C}{\partial x} = 0$. Note Equation (25) is a necessary condition for LCM instead of a sufficient condition. Mathematically, $\frac{\partial C}{\partial x} = 0$ means that chlorophyll-a reaches local maxima or local minima in space. While there may exist multiple local maxima, the chlorophyll-a maximum is only one of them with maximum value. Biologically, Equation (25) means that phytoplankton growth rate is balanced by its loss rate, and an equilibrium state is reached locally. Beyond the region $(x = x_m)$, the chlorophyll-a concentration will increase (or decrease) towards either side. For example, deviated from the location of LCM, when $x < x_m/x > x_m$, the chlorophyll-a is always smaller than the maximum chlorophyll-a concentration at $x = x_m$ as the net growth rate μ_{net} is larger/smaller than zero.

Equation (25) means that the condition for LCM is only biologically controlled. Basically, this states that the maximum chlorophyll-a concentration in an aquatic system should be only limited by biological factors such as nutrient concentrations and light condition. It represents the capacity of the system for phytoplankton growth, which is not related to flow condition. On the other hand, the location of LCM can be influenced by physical factors, which is different from the condition of LCM. For example, if phytoplankton needs certain time to increase to its maximum concentration under a constant net growth, larger river flow will cause the maximum chlorophyll-a concentration occurring further downstream as water parcel with larger velocity can travel further for a given period. In the case when river flow is too large, maximum concentration may never be reached before the water parcel is advected out of the system, which partially explains why chlorophyll-a remained low in 2003 and 2004 in the TFR of James River (Figure 10).

If the expression of the net growth rate $\mu_{net}(x)$ is known, we can find the location of LCM by simply analyzing $\mu_{net}(x)$. However, in reality, $\mu_{net}(x)$ is often unknown. In order to estimate the location of LCM (or the location of maximum chlorophyll-a concentration in the TFR system), we can use Equations (12) by assuming:

- a. The river cross section has a shape $A = A_0 \cdot (1 + \alpha \cdot x)$ in the longitudinal direction and the velocity is $u(x) = \frac{Q}{A_0 \cdot (1 + \alpha \cdot x)}$, where A is the river cross section area; A_0 is the area at the boundary; Q is a constant river flow rate; and α is the coefficient to represent the longitudinal change of river cross section that can be positive, zero, or negative.
- b. Boundary condition of chlorophyll-a concentration a is constant.

688

689

690

691

- c. Phytoplankton net growth μ_{net} is constant before the location of LCM (beyond the LCM, it will become negative).
 - d. The maximum chlorophyll-a concentration is C_m , which is determined by biological factors related to the system capacity for phytoplankton growth. According to Equation (3), the corresponding accumulative growth at LCM is $G_m = \ln\left(\frac{C_m}{a}\right)$.
- Based on these assumptions and Equations (12), we can calculate the accumulative growth:

$$G = \begin{cases} \mu_{net} \cdot \int_0^x \frac{d\eta}{u(\eta)} = \mu_{net} \cdot \int_0^x \frac{A_0 \cdot (1 + \alpha \cdot \eta)}{Q} d\eta = \frac{\mu_{net} \cdot A_0}{2\alpha Q} \left[(1 + \alpha x)^2 - 1 \right], & \alpha \neq 0 \\ \frac{\mu_{net} \cdot A_0}{Q} x, & \alpha = 0 \end{cases}$$
(26)

693 At the location of LCM, we have $G(x_m) = G_m$, which leads to:

$$x_{m} = \begin{cases} \frac{1}{\alpha} \left(\sqrt{1 + 2\alpha\theta} - 1 \right), & \alpha \neq 0. \\ \theta, & \alpha = 0 \end{cases}$$
 (27)

where x_m is the location of LCM and $\theta = \frac{G_m Q}{A_0 \mu_{net}}$. Figure 13 shows the location of LCM predicted by Equation (27) with different α values for different shapes of river cross-sections. When θ increases, the location of LCM increases (moving towards downstream). Also, it is interesting to notice that the line curves upward/downward when $\alpha > 0/\alpha < 0$, while it is a straight line when $\alpha = 0$.

Equation (27) demonstrates that the location of LCM increases with river flow Q when other factors remain unchanged, which is consistent with the analysis above. To verify this, we extracted the locations of LCM from dataflow data in the TFR of James River and associated them with James River flow rates averaged for the past week. It well reproduces the relation between river flow and location of LCM that location of LCM moves downstream as river flow increases (Figure 14). In addition, a theoretical fit with positive α based on Equation (27) is shown in Figure 14. It matches the observational data well regarding the general trend. The upward curve with positive α is also consistent with the James River geomorphology in the TFR where river cross section generally increases from Station TF5.3 to Station TF5.5A (Figure 6). Despite of the simplicity of Equation (27), the good agreement between observation and theory suggests that our analytical model well represents the phytoplankton dynamics in the TFR of James River.

4.3 Extension to Three Dimensional System

In this work, the analytical model is only applied to one phytoplankton species in a one-dimensional system in the TFR. The concept of integrating physical processes and biological processes in phytoplankton dynamics may work for multiple phytoplankton species in three dimensional system if there is no species interaction. This extension is valid in an advection-dominant system (Cianelli et al., 2017), but may fails when physical mixing is too strong or too complicated. Cianelli et al. (2017)Assuming the three dimensional velocity field $\bar{u}(t,\bar{x})$ and net growth rate $\mu_{net}(t,\bar{x})$ (or $\mu_{net}^0(t,\bar{x})$) are known, the equation for the phytoplankton dynamics is:

$$\frac{\partial C}{\partial t} + \vec{u} \cdot \nabla C = \mu_{net} \cdot C, \quad \vec{x} \in V.$$
 (28)

719 Similar to Equation (3), the solution is:

$$C(t, \vec{x}) = a(t - T(t, \vec{x}), \vec{x}_0) \cdot e^{G(t, \vec{x})}, \qquad (29)$$

and water age $T(t, \bar{x})$ and accumulative growth are determined by following equations:

$$\frac{\partial T}{\partial t} + \vec{u} \cdot \nabla T = 1 \quad , \tag{30}$$

$$\frac{\partial G}{\partial t} + \bar{u} \cdot \nabla G = \mu_{net} \quad , \tag{31}$$

$$T(t, \vec{x}) = 0, \quad \vec{x} \in \Omega \quad , \tag{32}$$

$$G(t, \vec{x}) = 0, \quad \vec{x} \in \Omega \quad ,$$
 (33)

where Ω is the boundary on domain V; $a(t, \vec{x})$ is the boundary condition of phytoplankton concentration on Ω ; and \vec{x}_0 is the starting point on the boundary for water parcels. Note that the boundary Ω here does not refer to the physical surface that embraces the volume V, but refers to the location from which the water flow starts. If the feedback mechanism is added as $\mu_{net} = \mu_{net}^0 \cdot (1 + kC)$, the solution becomes:

$$C(t,x) = \frac{a(t-T, \vec{x}_0) \cdot e^G}{1 + k \cdot a(t-T, \vec{x}_0) \cdot (1 - e^G)},$$
(34)

vith a modified accumulative growth as shown below:

$$\frac{\partial G}{\partial t} + \vec{u} \cdot \nabla G = \mu_{net}^0 \ . \tag{35}$$

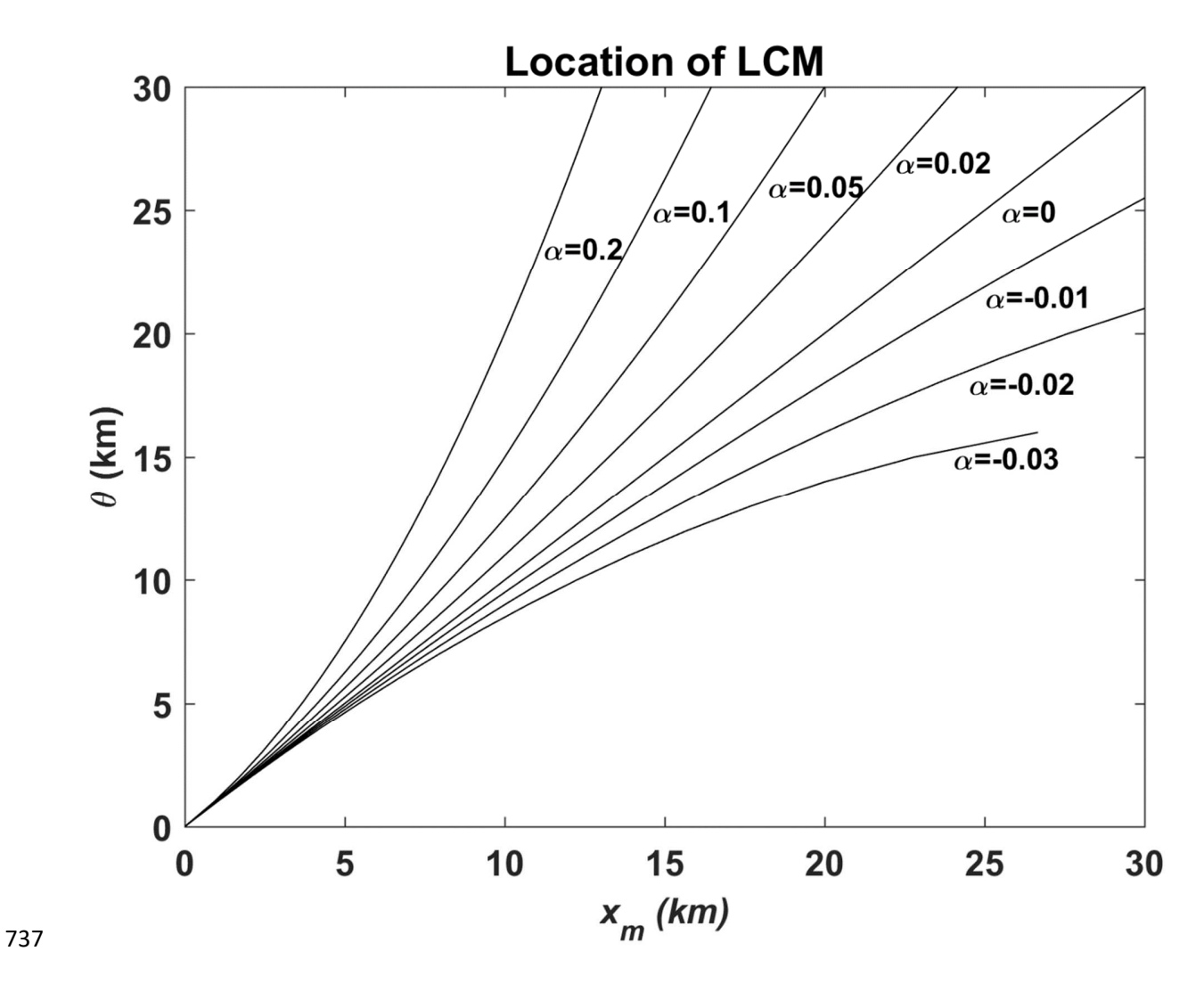


Figure 13. Location of LCM predicted by Equation (27) with different values of α (km⁻¹), where α represents the coefficient for longitudinal change of river cross section. The y-axis is $\theta = \frac{G_m Q}{A_0 \mu_{net}}$, where G_m is accumulative growth; Q is the river flow rate; and A_0 is the cross section area at the boundary.

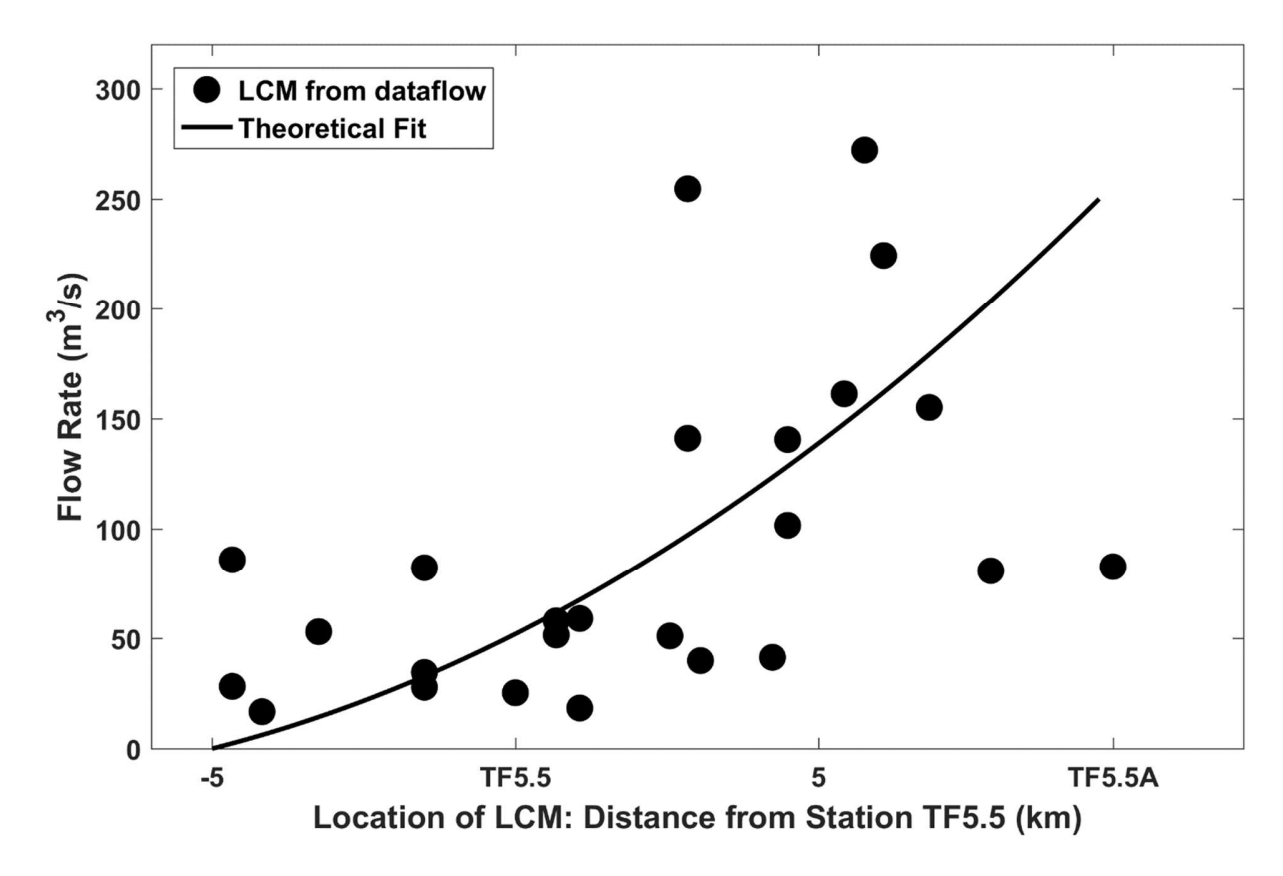


Figure 14. Location of LCM versus James River flow rate. Dots represent the LCM extracted from dataflow observational data in the TFR of James River, while the line is a theoretical fit based on G_m and G_m and G_m are G_m are G_m are G_m are G_m are G_m and G_m are G_m and G_m are G_m are G_m are G_m are G_m are G_m and G_m are G_m are

Equation (27) with $\frac{G_m}{A_0 \cdot \mu_{net}} = 150 \text{ s.m}^{-2} \text{ and } \alpha = 0.2 \text{ km}^{-1}$.

5 Summary

The combination of physical processes and biological processes influences phytoplankton in time and space. In this work, they are mathematically summarized into velocity field and phytoplankton net growth rate respectively to construct an analytical model for phytoplankton dynamics in a one-dimensional system. We are able to get an analytical solution for the downstream phytoplankton concentration. In order to account for the nonlinear biological processes that affect phytoplankton variation, we also provide an alternative solution with nonlinear reaction term. The nonlinear reaction term can also be used to approximate physical mixing. The analytical solutions have two essential components: water age and accumulative

growth. Both components have clear physical meanings providing insights on how physical and biological factors regulate the phytoplankton spatiotemporal variations. The analytical solution not only predicts downstream phytoplankton concentration based on boundary condition, but also provides a tool for us to integrate different types of field phytoplankton observations. We applied the analytical model in the TFR of James under different dynamic conditions. The good agreement between model results and observations validates the theory. In addition, based on the analytical solution, an analysis is made to study the LCM in the TFR. It shows that the condition of LCM is biologically controlled, but its location is related to river flow and river geomorphology.

In summary, the analytical model is useful in describing the phytoplankton dynamics in a onedimensional, advection-dominant system. It can be applied:

- a) to study the interaction between physical and biological factors on phytoplankton,
- b) to simulate downstream phytoplankton concentration in time and space,
- c) to analyze phytoplankton related phenomena such as LCM in estuary,
- d) and to approximate the nonlinear effects on phytoplankton growth.

771 Appendix A: Proof of Equation (9) as the solution to Equation (8)

Substituting Equation (9) into Equation (8), we have:

$$RHS = \frac{a \cdot \left(1 - \frac{\partial T}{\partial t}\right) \cdot e^{G} + a \cdot e^{G} \cdot \frac{\partial G}{\partial t}}{1 + k \cdot a \cdot \left(1 - e^{G}\right)} - \frac{a \cdot e^{G} \left[k \cdot a \cdot \left(1 - \frac{\partial T}{\partial t}\right) \cdot \left(1 - e^{G}\right) - k \cdot a \cdot e^{G} \cdot \frac{\partial G}{\partial t}\right]}{\left[1 + k \cdot a \cdot \left(1 - e^{G}\right)\right]^{2}}$$

$$+ u \frac{a \cdot \left(-\frac{\partial T}{\partial x}\right) \cdot e^{G} + a \cdot e^{G} \cdot \frac{\partial G}{\partial x}}{1 + k \cdot a \cdot \left(1 - e^{G}\right)} - u \frac{a \cdot e^{G} \left[k \cdot a \cdot \left(-\frac{\partial T}{\partial x}\right) \cdot \left(1 - e^{G}\right) - k \cdot a \cdot e^{G} \cdot \frac{\partial G}{\partial x}\right]}{\left[1 + k \cdot a \cdot \left(1 - e^{G}\right)\right]^{2}}$$

$$= \frac{a \cdot \left(1 - \frac{\partial T}{\partial t} - u \frac{\partial T}{\partial x}\right) \cdot e^{G} + a \cdot e^{G} \cdot \left(\frac{\partial G}{\partial t} + u \frac{\partial G}{\partial x}\right)}{1 + k \cdot a \cdot \left(1 - e^{G}\right)}$$

$$- \frac{a \cdot e^{G} \left[k \cdot a \cdot \left(1 - \frac{\partial T}{\partial t} - u \frac{\partial T}{\partial x}\right) \cdot \left(1 - e^{G}\right) - k \cdot a \cdot e^{G} \cdot \left(\frac{\partial G}{\partial t} + u \frac{\partial G}{\partial x}\right)\right]}{\left[1 + k \cdot a \cdot \left(1 - e^{G}\right)\right]^{2}}$$

$$= \frac{a \cdot e^{G} \cdot \mu_{net}^{0}}{1 + k \cdot a \cdot \left(1 - e^{G}\right)} + \frac{k \cdot a^{2} \cdot e^{2G} \cdot \mu_{net}^{0}}{\left[1 + k \cdot a \cdot \left(1 - e^{G}\right)\right]^{2}}$$

$$= \mu_{net}^{0} \cdot C + \mu_{net}^{0} \cdot k \cdot C^{2} = LHS$$

Note that Equations (4, 10) are used in the above derivation.

Appendix B: Calculation of Net Growth Rate in the TFR of James River

In this section, the phytoplankton net growth rate from 1999 to 2005 is estimated based on the water quality measurements from Chesapeake Bay Program (2016) and water quality model formulations from Park et al. (1995). First, the spatiotemporal variations of nutrients (NO₃, NH₄, PO₄), temperature and light attenuation coefficient are estimated by linearly interpolating the measurement data onto time period [01/01/1999, 12/31/2005] and space range [0 km, 65 km] (Figure 6). The results are shown in Figure B1. In addition, the solar radiation from North American Regional Reanalysis (NARR) is used to estimate Photosynthetically Available Radiation (PAR) for phytoplankton growth (Figure). The daytime variation is calculated based on latitude and day number of year (Forsythe et al., 1995).

The information obtained above is then used to compute phytoplankton net growth rate following Park et al. (1995) and Chapra (1997). The net growth of phytoplankton is composed of its growth, basal metabolism and predation by higher trophic levels with the expression:

$$\mu_{net} = G - BM - PR . \tag{B1}$$

788 where *G* is growth rate (day⁻¹), *BM* is metabolism rate (day⁻¹) and *PR* is the predation rate (day⁻¹).

The growth rate represents how phytoplankton grows in the environment of nutrients, light and temperature as below:

$$G = G_{\text{max}} \cdot f(N) \cdot f(I) \cdot f(T). \tag{B2}$$

$$f(N) = \min\left(\frac{NO_3 + NH_4}{KHN + NO_3 + NH_4}, \frac{PO_4}{KHP + PO_4}\right).$$
 (B3)

$$f(I) = \frac{1}{H} \int_0^H \frac{I}{I_m} \exp\left(-\frac{I}{I_m} + 1\right) \cdot dz.$$
 (B4)

$$I = I_0 \cdot \exp(-Ke \cdot Z). \tag{B5}$$

$$f(T) = \begin{cases} e^{-KTG1 \cdot \left(T_{opt} - T\right)^2, \text{ if } T \leq T_{opt}} \\ e^{-KTG2 \cdot \left(T - T_{opt}\right)^2, \text{ if } T > T_{opt}} \end{cases}$$
(B6)

where G_{\max} is the maximum growth rate (day⁻¹); [f(N), f(I), f(I), f(T)] are the phytoplankton growth limitation factors for nutrients, light and temperature respectively; NO_3 is nitrate concentration (mg/L); NH_4 is ammonium concentration (mg/L); PO_4 is phosphate concentration (mg/L); KHN (mg/L) and KHP (mg/L) are the half saturation constants for nitrogen and phosphorus respectively; I is light intensity (Ly/day) and I_0 is the light intensity (Ly/day) at water surface; I_m is the optimal light intensity (Ly/day) for phytoplankton growth; Ke is light extinction

coefficient (m⁻¹); H is water depth (m); Z is the vertical distance from water surface (m); T is water temperature (°C) and T_{opt} is the optimal temperature for phytoplankton growth (°C); KTG1 (°C⁻²) and KTG2 (°C⁻²) are the temperature dependence coefficients for phytoplankton growth when temperature is blow and above T_{opt} respectively.

The metabolism rate and predation rate are both modulated by temperature as below:

$$BM = BM_0 \cdot \exp \left[KT \cdot \left(T - TR \right) \right]. \tag{A7}$$

$$PR = PR_0 \cdot \exp\left[KT \cdot (T - TR)\right]. \tag{A8}$$

where $BM_0(\text{day}^{-1})$ and $PR_0(\text{day}^{-1})$ are the reference metabolism rate and predation rate at reference temperature TR (°C) respectively; KT is the temperature dependence coefficient (°C⁻¹).

Based on Equations (B1-A8), we computed phytoplankton net growth rate μ_{net} that varies from 1999 to 2005 in our model domain (Figure 6) with parameter values in Table B1 referenced to Park et al. (1995).



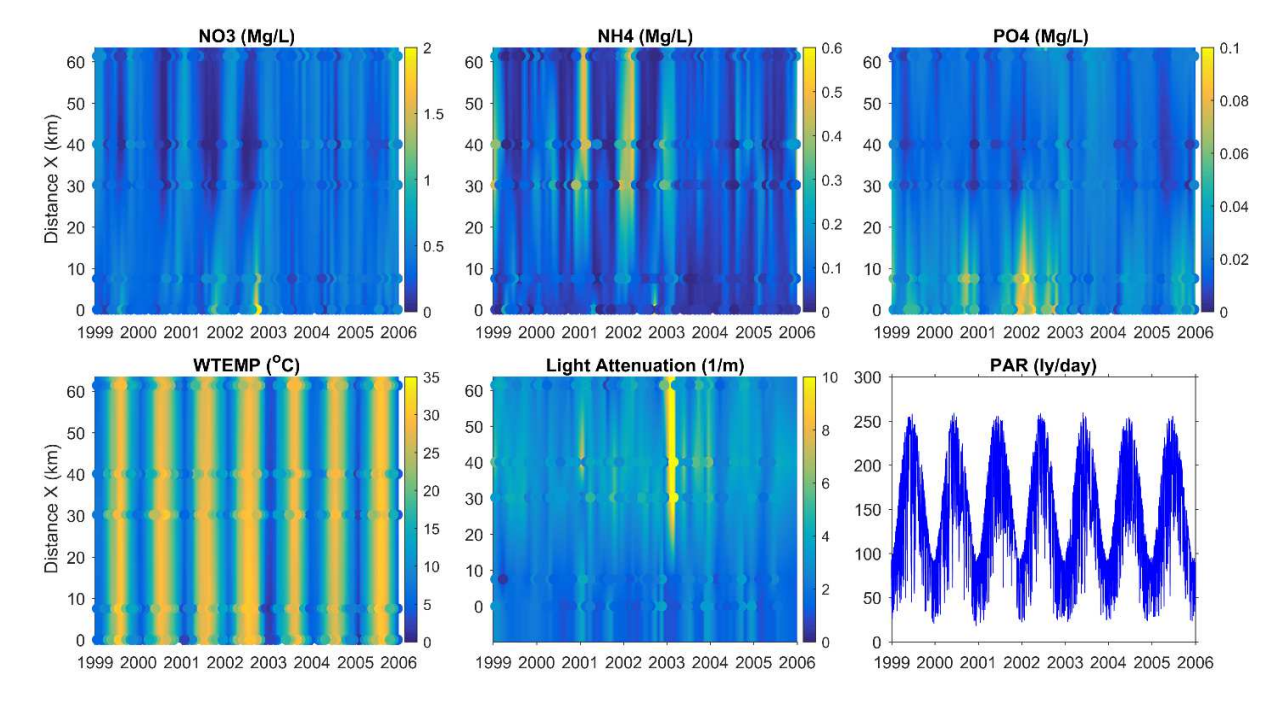


Figure B1. The interpolated NO₃, NH₄, PO₄, water temperature, and light attenuation coefficient based on monthly observational data that are shown in dots. The lower right panel is daily mean

Photosynthetically Available Radiation in unit of Langley/day extracted from North American Regional Reanalysis database.

Table B1. Parameter values used to calculate phytoplankton net growth rate

$G_{\text{max}} = 3.0 \text{ day}^{-1}$	<i>KHN</i> =0.01 mg/L	<i>KHP</i> =0.001 mg/L	$I_m = 40 \text{ Ly/day}$
KTG1=0.001 °C ⁻¹	KTG2=0.001 °C ⁻¹	T_{opt} =25 °C	$BM_0 = 0.04 \text{ day}^{-1}$
$PR_0 = 0.01 \text{ day}^{-1}$	$KT = 0.069 ^{\circ}\text{C}^{-1}$	<i>TR</i> =20 °C	

Appendix C: Flow Rate of James River

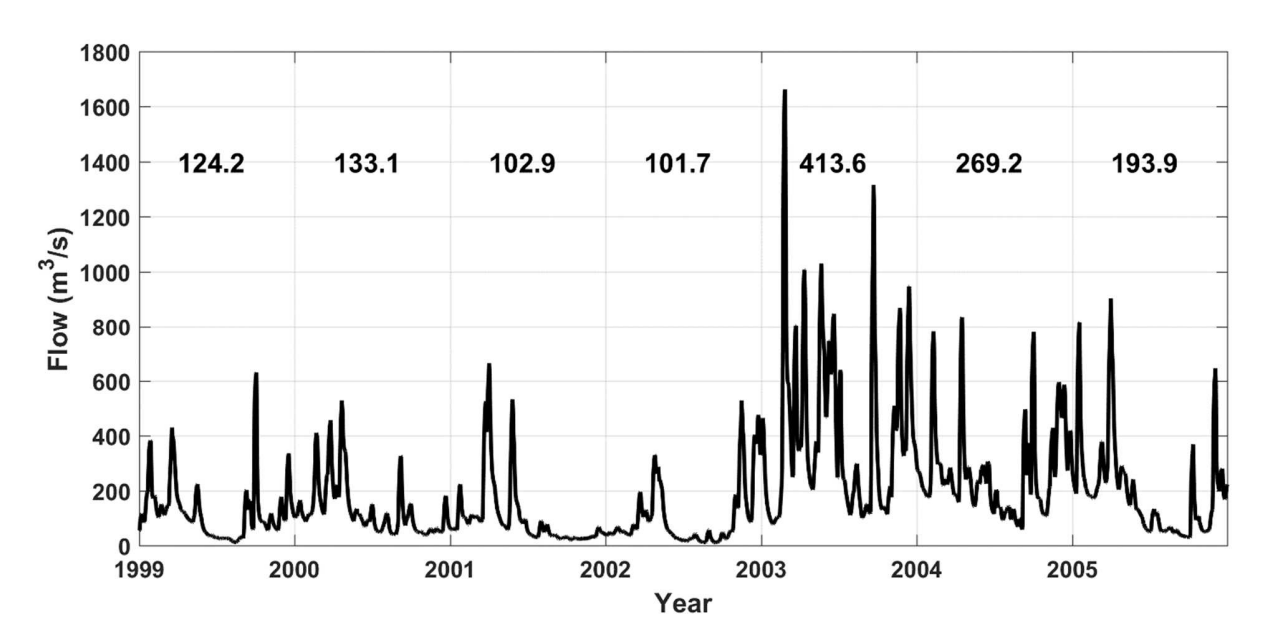


Figure C1. James River flow rate from 1999 to 2005. The number on the figure for each year is annual mean river flow rates. River flow data is from U.S. Geological Survey Data (2018).

Acknowledgement

This study was funded by DOE project 'Improving tide-estuary representation in MPASOcean' with program grant number DE-SC0016263 (to Zhang Yinglong at Virginia Institute of
Marine Sciences).

851

852

853

854

855

856

864

867

868

869

870

871

- Anderson, D. M., Burkholder, J. M., Cochlan, W. P., Glibert, P. M., Gobler, C. J., Heil, C. A., . . . Vargo, G. A. (2008). Harmful algal blooms and eutrophication: Examining linkages from selected coastal regions of the United States. *Harmful Algae*, 8(1), 39-53. doi:10.1016/j.hal.2008.08.017
- Anderson, D. M., Cembella, A. D., & Hallegraeff, G. M. (2012). Progress in Understanding Harmful Algal Blooms: Paradigm Shifts and New Technologies for Research, Monitoring, and Management. *Annual Review of Marine Science, Vol 4, 4*, 143-176. doi:10.1146/annurev-marine-120308-081121
- Barros, M., Pedersén, M., Colepicolo, P., & Snoeijs, P. (2003). Self-shading protects phytoplankton communities against H2O2-induced oxidative damage. *Aquatic microbial ecology*, *30*(3), 275-282.
- Borsuk, M. E., Stow, C. A., & Reckhow, K. H. (2004). Confounding effect of flow on estuarine response to nitrogen loading. *Journal of Environmental Engineering-Asce*, 130(6), 605-614. doi:Doi 10.1061/(Asce)0733-9372(2004)13.:6(605)
 - Boynton, W. R., Kemp, W. M., & C.W., K. (1982). A comparative analysis of nutrients and other factors influencing estuarine phytoplankton production. V. S. Kennedy, ed. Estuarine comparisons. Academic, New York, 69-90.
 - Bukaveckas, P. A., Barry, L. E., Beckwith, M. J., David, V., & Lederer, B. (2011). Factors Determining the Location of the Chlorophyll Maximum and the Fate of Algal Production within the Tidal Freshwater James River. *Estuaries and Coasts*, *34*(3), 569-582. doi:10.1007/s12237-010-9372-4
- Carroll, S., Liu, A., Dawes, L., Hargreaves, M., & Goonetilleke, A. (2013). Role of Land Use and Seasonal Factors in Water Quality Degradations. *Water Resources Management*, 27(9), 3433-3440. doi:DOI 10.1007/s11269-013-0356-6
- Cerco, C. F. (2013). Modeling the pH in the tidal fresh Potomac River under conditions of varying
 hydrology and loads.
- Cerco, C. F., & Noel, M. R. (2004). The 2002 Chesapeake Bay Eutrophication Model. *Prepared* for: Chesapeake Bay Program Office, U.S. Environmental Protection Agency.
 - Chapra, S. C. (1997). Surface Water Quality Modeling. McGraw-Hill, New York, .
- Chesapeake Bay Program. (2016). Chesapeake Bay program water quality database 1984–present. *Retrieved from: http://www.chesapeakebay.net/data/downloads*.
 - Chesapeake Environmental Communications. (2015). Modeling Support for the James River Chlorophyll Study, Task 2 Empirical Data Analysis Report. *Prepared for: Commonwealth of Virginia Department of Environment Quality, https://www.deq.virginia.gov/Portals/0/DEQ/Water/WaterQualityStandards/James%20River%20Chl%20A%20Study/SAP_Reports/James%20Modeling%20Data%20Summary%20Report-CEC-2012.pdf.*
- Cianelli, D., D'Alelio, D., Uttieri, M., Sarno, D., Zingone, A., Zambianchi, E., & d'Alcalà, M. R. (2017). Disentangling physical and biological drivers of phytoplankton dynamics in a coastal system. *Scientific reports*, 7(1), 15868.
- Cloern, J. E. (1987). Turbidity as a control on phytoplankton biomass and productivity in estuaries. *Continental Shelf Research*, 7(11-12), 1367-1381. doi:10.1016/0278-4343(87)90042-2

- Cloern, J. E. (1996). Phytoplankton bloom dynamics in coastal ecosystems: A review with some general lessons from sustained investigation of San Francisco Bay, California. *Reviews of Geophysics*, 34(2), 127-168. doi:Doi 10.1029/96rg00986
- Cloern, J. E. (2006). Habitat connectivity and ecosystem productivity: Implications from a simple model. *The American Naturalist*, *169*(1), E21-E33.
- Deleersnijder, E., Campin, J. M., & Delhez, E. J. M. (2001). The concept of age in marine modelling I. Theory and preliminary model results. *Journal of Marine Systems*, 28(3-4), 229-267. doi:Doi 10.1016/S0924-7963(01)00026-4
- Du, J., & Shen, J. (2015). Decoupling the influence of biological and physical processes on the dissolved oxygen in the Chesapeake Bay. *Journal of Geophysical Research: Oceans*, 120(1), 78-93.
- Dugdale, R. C., Wilkerson, F. P., & Parker, A. E. (2016). The effect of clam grazing on phytoplankton spring blooms in the low-salinity zone of the San Francisco Estuary: A modelling approach. *Ecological Modelling*, 340, 1-16.
- Fang, C. S., Kuo, A. Y., Hyer, P. V., & Hargis, J. W. J. (1973). Hydrography and hydrodynamics of Virginia estuaries. IV. Mathematical Model Studies of Water Quality in the James Estuary. Speical report No. 41, Virginia Institute of Marine Science, September.
- Federal Emergency Management Agency. (2010). Procedure Memorandum No. 61, Standards for LiDAR and Other High Quality Digital Topography, September 27, 2010.

898

899

900 901

902

903

904 905

906 907

- Filardo, M. J., & Dunstan, W. M. (1985). Hydrodynamic Control of Phytoplankton in Low Salinity Waters of the James River Estuary, Virginia, USA. *Estuarine Coastal and Shelf Science*, 21(5), 653-667. doi:Doi 10.1016/0272-7714(85)90064-2
- Fitzpatrick, J., Kogan, N., & Mahwah, N. (2014). Modeling in Support of the James River Chlorophyll Study. *Chesapeake Bay Modeling symposium, in Annapolis, MD, 2014, http://communitymodeling.org/chesapeakemeetings/CheMS2014/presentations/96/498.pd f.*
- Flynn, K. J., & Mitra, A. (2009). Building the "perfect beast": modelling mixotrophic plankton. *Journal of Plankton Research*, *31*(9), 965-992.
- Forsythe, W. C., Rykiel, E. J., Stahl, R. S., Wu, H.-i., & Schoolfield, R. M. (1995). A model comparison for daylength as a function of latitude and day of year. *Ecological Modelling*, 80(1), 87-95.
- Glibert, P. M., Magnien, R., Lomas, M. W., Alexander, J., Fan, C. L., Haramoto, E., . . . Kana, T. M. (2001). Harmful algal blooms in the Chesapeake and coastal bays of Maryland, USA: Comparison of 1997, 1998, and 1999 events. *Estuaries*, 24(6A), 875-883. doi:Doi 10.2307/1353178
- Heisler, J., Glibert, P. M., Burkholder, J. M., Anderson, D. M., Cochlan, W., Dennison, W. C., . .
 Suddleson, M. (2008). Eutrophication and harmful algal blooms: A scientific consensus. *Harmful Algae*, 8(1), 3-13. doi:DOI 10.1016/j.hal.2008.08.006
- Hong, B., & Shen, J. (2013). Linking dynamics of transport timescale and variations of hypoxia in
 the Chesapeake Bay. *Journal of Geophysical Research-Oceans*, 118(11), 6017-6029.
 doi:Doi 10.1002/2013jc008859
- James, F., DI TORO, D. M., & WU, K. B. (1992). Bloom of Microcystis Aeruginosa in the Upper Potomac River Estuary: Interactions between Primary Productivity, pH and Sediment Phosphorus Release.

- Kemp, W. M., & Boynton, W. R. (1992). Benthic-pelagic interactions: nutrient and oxygen dynamics. Oxygen Dynamics in the Chesapeake Bay: A synthesis of Recent Research.
 Maryland Sea Grant Book, College Park, MD, 149-221.
- Li, C., Valle-Levinson, A., Atkinson, L. P., Wong, K. C., & Lwiza, K. M. (2004). Estimation of drag coefficient in James River Estuary using tidal velocity data from a vessel-towed
 ADCP. *Journal of Geophysical Research: Oceans, 109*(C3).
- Lim, A. S., Jeong, H. J., Jang, T. Y., Jang, S. H., & Franks, P. J. S. (2014). Inhibition of growth rate and swimming speed of the harmful dinoflagellate Cochlodinium polykrikoides by diatoms: Implications for red tide formation. *Harmful Algae*, *37*, 53-61. doi:DOI 10.1016/j.hal.2014.05.003
- Liu, Q., Chai, F., Dugdale, R., Chao, Y., Xue, H., Rao, S., . . . Wang, Z. (2018). San Francisco
 Bay Nutrients and Plankton Dynamics as Simulated by a Coupled Hydrodynamic Ecosystem Model. *Continental Shelf Research*.
- Lucas, L. V., Thompson, J. K., & Brown, L. R. (2009). Why are diverse relationships observed
 between phytoplankton biomass and transport time? *Limnology and Oceanography*, 54(1),
 381-390. doi:DOI 10.4319/lo.2009.54.1.0381
- 938 MacCready, P., & Geyer, W. R. (2010). Advances in Estuarine Physics. *Annual Review of Marine* 939 *Science*, 2, 35-58. doi:10.1146/annurev-marine-120308-081015
- 940 Marshall, H. G., & Affronti, L. F. (1992). Seasonal phytoplankton development within three rivers 941 in the lower Chesapeake Bay Region. *Virginia Journal of Science, 43, Number 1A*.

943 944

945

946

947

948 949

950 951

952

953

- Morse, R. E., Mulholland, M. R., Hunley, W. S., Fentress, S., Wiggins, M., & Blanco-Garcia, J. L. (2013). Controls on the initiation and development of blooms of the dinoflagellate Cochlodinium polykrikoides Margalef in lower Chesapeake Bay and its tributaries. *Harmful Algae*, 28, 71-82. doi:DOI 10.1016/j.hal.2013.05.013
- Muylaert, K., Tackx, M., & Vyverman, W. (2005). Phytoplankton growth rates in the freshwater tidal reaches of the Schelde estuary (Belgium) estimated using a simple light-limited primary production model. *Hydrobiologia*, *540*, 127-140. doi:10.1007/s10750-004-7128-5
- Park, K., Kuo, A. Y., Shen, J., & Hamrick, J. M. (1995). A Three-Dimensional Hydrodynamic-Eutrophication (HEM-3D): Description of Water Quality and Sediment Process Submodels. Special Report in Applied Marine Science and Ocean Engineering NO. 327.
 - Pennock, J. R. (1985). Chlorophyll distributions in the Delaware estuary: regulation by light-limitation. *Estuarine, Coastal and Shelf Science, 21*(5), 711-725.
- 955 Qin, Q., & Shen, J. (2017). The contribution of local and transport processes to phytoplankton 956 biomass variability over different timescales in the Upper James River, Virginia. *Estuarine*, 957 *Coastal and Shelf Science*, 196, 123-133.
- Ralston, D. K., Brosnahan, M. L., Fox, S. E., Lee, K. D., & Anderson, D. M. (2015). Temperature
 and Residence Time Controls on an Estuarine Harmful Algal Bloom: Modeling
 Hydrodynamics and Alexandrium fundyense in Nauset Estuary. *Estuaries and Coasts*,
 38(6), 2240-2258. doi:10.1007/s12237-015-9949-z
- 962 Rice University. (2013). Biology, textbox funded by OpenStax. 963 https://openstax.org/details/books/biology.
- 964 Sellner, K. G., R.V.Lacouture, & C.R.Parrish. (1988). Effects of increasing salinity on a cyanobacteria bloom in the Potomac River estuary *Journal of Plankton Research*, *10 no.* 1, 49-61.

- Shen, J., Boon, J. D., & Kuo, A. Y. (1999). A modeling study of a tidal intrusion front and its impact on larval dispersion in the James River estuary, Virginia. *Estuaries*, 22(3A), 681-692. doi:Doi 10.2307/1353055
- 970 Shen, J., Hong, B., & Kuo, A. Y. (2013). Using timescales to interpret dissolved oxygen distributions in the bottom waters of Chesapeake Bay. *Limnology and Oceanography*, 58(6), 2237-2248. doi:DOI 10.4319/lo.2013.58.6.2237
- 973 Shen, J., & Lin, J. (2006). Modeling study of the influences of tide and stratification on age of 974 water in the tidal James River. *Estuarine Coastal and Shelf Science*, 68(1-2), 101-112. 975 doi:10.1016/j.eccs.2006.01.014
- 976 Shen, J., Wang, R., Qu, Q., & Sisson, M. (2016a). The Interaction of Hydrodynamics and 977 Phytoplankton Bloom in the TidalJames River, Virginia. *Chesapeake Bay Modeling* 978 *symposium, June 1st, 2016, in Willsmsburg*.
- 979 Shen, J., Wang, R., & Sisson, M. (2016b). James River Watershed Model, Development of 980 Hydrodynamic Model. *Prepared for Virginia Department of Environmental Quality*, 629 981 *East Main Street, Richmond, VA 23219*.

983

984 985

986

989 990

991

1007

- Shen, J., Wang, R., & Sisson, M. (2017). Assessment of Hydrodynamic and Water Quality Impacts for Channel Deepening in the Thimble Shoals, Norfolk Harbor, And Elizabeth River Channels. *Special Report No. 454 In Applied Marine Science and Ocean Engineering, doi:10.21220/V5R41Z*, (https://www.nao.usace.army.mil/Portals/31/docs/civilworks/Nrflk HrbrDeepening/SRAMSOE_454_sep2017.pdf).
- 987 Sze, P. (1981). A culture model for phytoplankton succession in the Potomac River near Washington, DC (USA). *Phycologia*, 20(3), 285-291.
 - U.S. Geological Survey Data. (2018). National Water Information System data available on the World Wide Web (USGS Water Data for the Nation), accessed [June 10, 2018], at URL https://waterwatch.usgs.gov.
- Wang, C.-F., & Y.Kuo, A. (2009). The development of an Integrated Model (TORI-WQM) for the
 Water Quality and Plankton Dynamics in the Estuaries and Coastal Seas of Taiwan. *Taiwan* Ocean Reserach Institute, National Applied Research Laboratories.
- 995 Willmott, C. J. (1981). On the validation of models. *Physical geography*, 2(2), 184-194.
- Wood, J., Bukaveckas, P., Garman, G., & McIninch, S. (2013). Causes and Consequences of Algal
 Blooms in the Tidal Freshwater James River. Report to Virginia Department of
 Environmental Quality.
- Ye, F., Zhang, Y., Wang, H. V., Friedrichs, M. A., Irby, I. D., Alteljevich, E., . . . Shen, J. (2018).
 A 3D unstructured-grid model for Chesapeake Bay: Importance of bathymetry. *Ocean Modelling*, 127, 16-39.
- Zhang, Y., & Baptista, A. M. (2008). SELFE: A semi-implicit Eulerian-Lagrangian finite-element model for cross-scale ocean circulation. *Ocean Modelling*, 21(3-4), 71-96. doi:DOI 10.1016/j.ocemod.2007.11.005
- Zhang, Y., Ye, F., Stanev, E. V., & Grashorn, S. (2016). Seamless cross-scale modeling with
 SCHISM. *Ocean Modelling*, 102, 64-81. doi:10.1016/j.ocemod.2016.05.002